

# ICT–Isomerization-Induced Turn-On Fluorescence Probe with a Large Emission Shift for Mercury Ion: Application in Combinational Molecular Logic

Sushil Ranjan Bhatta,<sup>†</sup> Bijan Mondal,<sup>‡</sup> Gonela Vijaykumar,<sup>§</sup> and Arunabha Thakur<sup>\*,†,‡,⊥</sup>

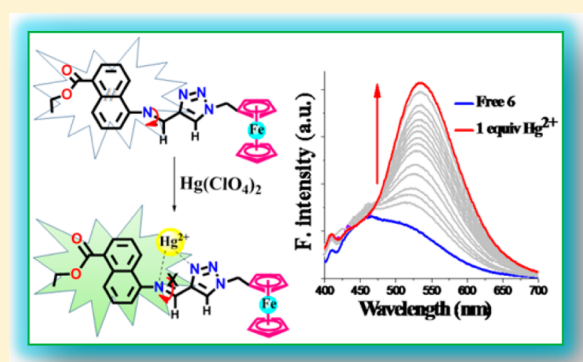
<sup>†</sup>Department of Chemistry, National Institute of Technology Rourkela, Rourkela-769 008, Odisha, India

<sup>‡</sup>Department of Chemistry, Indian Institute of Technology Madras, Chennai-600 036, India

<sup>§</sup>Department of Chemical Science, Indian Institute of Science Education and Research Kolkata, Mohanpur-741 246, India

## Supporting Information

**ABSTRACT:** A unique turn-on fluorescent device based on a ferrocene–aminonaphtholate derivative specific for  $\text{Hg}^{2+}$  cation was developed. Upon binding with  $\text{Hg}^{2+}$  ion, the probe shows a dramatic fluorescence enhancement (the fluorescence quantum yield increases 58-fold) along with a large red shift of 68 nm in the emission spectrum. The fluorescence enhancement with a red shift may be ascribed to the combinational effect of  $\text{C}=\text{N}$  isomerization and an extended intramolecular charge transfer (ICT) mechanism. The response was instantaneous with a detection limit of  $2.7 \times 10^{-9}$  M. Upon  $\text{Hg}^{2+}$  recognition, the ferrocene/ferrocenium redox peak was anodically shifted by  $\Delta E_{1/2} = 72$  mV along with a “naked eye” color change from faint yellow to pale orange for this metal cation. Further, upon protonation of the imine nitrogen, the present probe displays a high fluorescence output due to suppression of the  $\text{C}=\text{N}$  isomerization process. Upon deprotonation using strong base, the fluorescence steadily decreases, which indicates that  $\text{H}^+$  and  $\text{OH}^-$  can be used to regulate the off–on–off fluorescence switching of the present probe. Density functional theory studies revealed that the addition of acid leads to protonation of the imine N (according to natural bond orbital analysis), and the resulting iminium proton forms a strong H-bond (2.307 Å) with one of the triazole N atoms to form a five-membered ring, which makes the molecule rigid; hence, enhancement of the ICT process takes place, thereby leading to a fluorescence enhancement with a red shift. The unprecedented combination of  $\text{H}^+$ ,  $\text{OH}^-$ , and  $\text{Hg}^{2+}$  ions has been used to generate a molecular system exhibiting the INHIBIT–OR combinational logic operation.



## INTRODUCTION

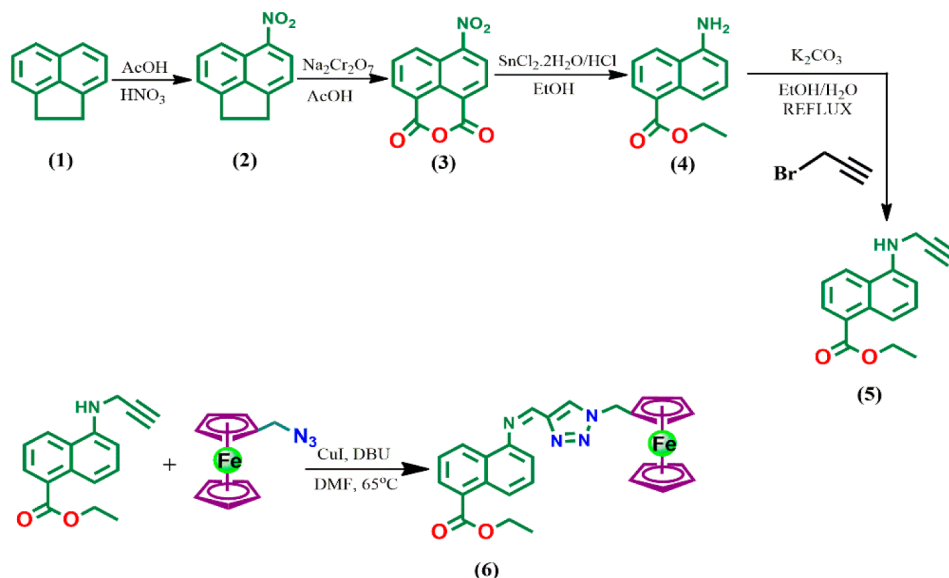
A wide range of molecular structures, chemical phenomena, and mechanisms can be marshaled to generate a variety of molecular logic operations according to the Boolean blueprint. Molecular logic gates, capable of performing Boolean logic operations in response to external stimuli such as physical, chemical, and biological inputs, are becoming an exciting trend in the forefront of research because of the growing demands of future information technology.<sup>1–4</sup> Following the pioneering work of de Silva in 1993,<sup>5</sup> a large number of molecular and supramolecular logic gates<sup>6–8</sup> based on organic molecules, nucleic acids, proteins, and micro- and nanomaterials have been successfully demonstrated over the last two decades.<sup>9–11</sup> However, it is still a great challenge to develop next-generation molecular logic gates based on new functional materials with potential applicability. Recently a tremendous development toward the exploitation of multiple and simple logic gates<sup>12,13</sup> such as OR, AND, and INHIBIT gates for the design of various smart materials have been documented.<sup>14–16</sup> The use of fluorescence signals in logic gates<sup>17–19</sup> has become a focus of extensive research interest because of their many advantages,

such as high sensitivity, rapid response, low background, and the capability of doing recognition in a nondestructive manner.

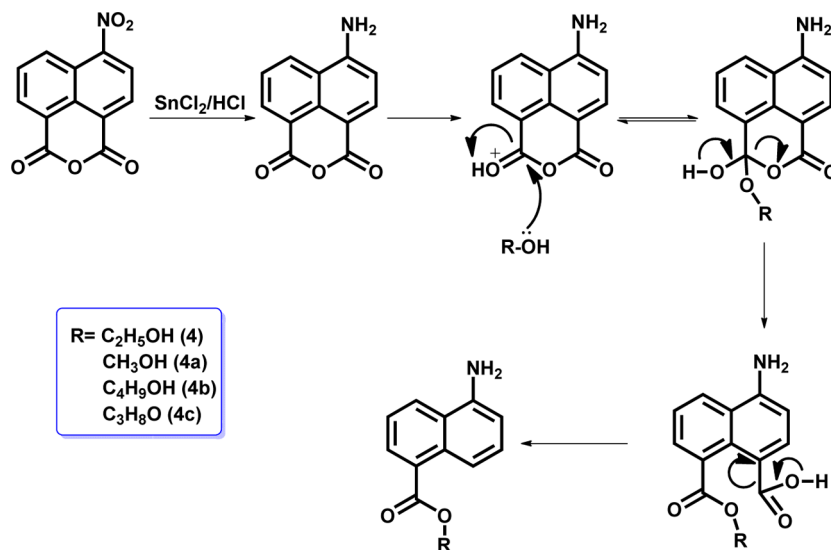
The development of highly sensitive and selective metal-ion-responsive fluorescent sensors for the efficient tracking of biologically and environmentally important metal ions is one of the vital goals for chemists.<sup>20</sup>  $\text{Hg}^{2+}$  ion is well-known for quenching the fluorescence of fluorophores via a spin–orbit coupling<sup>21</sup> and/or energy transfer mechanism.<sup>22</sup> Therefore, the design and synthesis of new “turn-on” fluorescent probes for  $\text{Hg}^{2+}$  ion based on novel interaction mechanisms between recognition and signal-reporting units is still an active research field. A variety of different signaling mechanisms, including photoinduced electron/energy transfer (PET),<sup>23</sup> metal-to-ligand charge transfer (MLCT),<sup>24</sup> intramolecular charge transfer (ICT),<sup>25</sup> excimer/excimer formation,<sup>26</sup> excited-state intra/intermolecular proton transfer (ESPT),<sup>27</sup> and fluorescence resonance energy transfer (FRET), etc., have been developed and extensively applied for the optical detection of

Received: May 23, 2017

Scheme 1. Synthesis of Compound 6



Scheme 2. Mechanism for the Formation of Compounds 4–4c

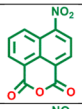
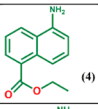
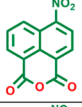
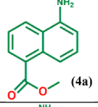
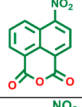
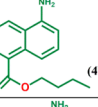
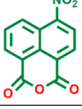
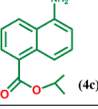


different species to date. Among these sensing mechanisms, the C=N isomerization process has been developed recently.<sup>28</sup> Compounds possessing C=N bonds are often nonfluorescent, since the C=N isomerization process is considered to be one of the major decay processes of excited states. The pioneer work by Wang and co-workers demonstrated that metal complexation to the C=N group (the complexation approach) can inhibit this nonradiative process, thereby leading to strong fluorescence emission.<sup>29</sup> Further, Guo and co-workers found that the intramolecular hydrogen bonding (the hydrogen bond approach)<sup>30</sup> also plays a crucial role in inhibition of the C=N isomerization process. However, fluorescence enhancement due to inhibition of C=N isomerization by metal complexation and protonation (hydrogen bonding) simultaneously has not been explored to date.

In the present work, we have developed triazole- and imine-tethered aminonaphthalene–ferrocene conjugate as a potential fluorescent sensing molecule for Hg<sup>2+</sup> ion. Our choice of the aminonaphthalene unit as the fluorophore arose from the fact

that it possesses excellent spectroscopic properties, such as good photostability, high fluorescence quantum yield, and tunable fluorescence emission. On the other hand, ferrocene is a very attractive building block because of its reversible redox property and its high stability in the presence of air and moisture. The two parts are linked by a triazole ring, a versatile recognition unit especially for transition metal cations,<sup>31,32</sup> and by a C=N bond. Therefore, the combination of aminonaphthalene and ferrocene units via a triazole ring and a C=N bond generates a molecular system where fluorescence can be modulated by controlling the C=N bond isomerization process through complexation or through protonation. Further, fluorescence modulation via protonation/deprotonation and metal complexation with the C=N bond have been judiciously applied to construct an INHIBIT–OR combinational logic gate for the first time.

Table 1

Sl. No.	Reactant	Product	Solvent	Reaction Procedure	Yields
1.		 (4)	Ethanol	SnCl <sub>2</sub> ·2H <sub>2</sub> O/ HCl, 2 h, Reflux.	67%
2.		 (4a)	Methanol	SnCl <sub>2</sub> ·2H <sub>2</sub> O/ HCl, 2 h, Reflux.	70%
3.		 (4b)	Butanol	SnCl <sub>2</sub> ·2H <sub>2</sub> O/ HCl, 3 h, Reflux.	65%
4.		 (4e)	Isopropanol	SnCl <sub>2</sub> ·2H <sub>2</sub> O/ HCl, 2.5 h, Reflux.	68%

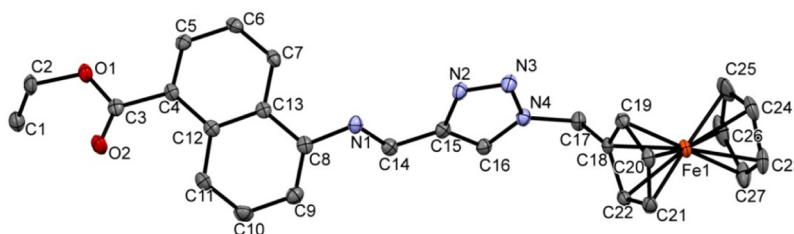


**Figure 1.** Molecular structure of **6** with thermal ellipsoids drawn at the 50% probability level. Selected bond lengths (Å) and angles (deg): C14–C15 1.457(3), C14–N1 1.277(3), N1–C8 1.422(3), O2–C3 1.206(3), C3–O1 1.350(3), N4–C17 1.472(3), [Triazole ring: C15–C16 1.378(3), C16–N4 1.342(3), N3–N4 1.352(3), N2–N3 1.311(3), N2–C15 1.367(3)]; N4–C17–C18 110.6(2), N1–C14–C15 121.3(2), C8–N1–C14 118.0(2), O1–C3–O2 122.7(2), C2–O1–C3 116.0(2), [Triazole ring N2–N3–N4 107.2(2), N3–N4–C16 111.2(2), N4–C16–C15 104.5(2), C16–C15–N2 108.3(2)].

## RESULTS AND DISCUSSION

**Synthesis of Compound 6.** Our attempts to synthesize 4-amino-1,8-naphthalic anhydride from 4-nitro-1,8-naphthalic anhydride under reducing conditions using SnCl<sub>2</sub>·2H<sub>2</sub>O and HCl led to the formation of compound **4** in good yield (Scheme 1). We tuned all of the possible reaction conditions to obtain aminonaphthalic anhydride, but all the reaction conditions, even at room temperature, afforded the decarboxylated product **4** in good yield. The formation of the product was confirmed by <sup>1</sup>H and <sup>13</sup>C NMR spectra, which clearly showed the presence of the ethyl moiety in compound **4**. A plausible mechanism for the formation of the product might be nucleophilic attack by ethanol to the carbonyl carbon C8 followed by decarboxylation (Scheme 2). In order to confirm the role of the solvent, we investigated the reactivity of several other solvents, including methanol, *n*-butanol, and isopropanol, and we indeed found that the alkyl part of the ester moiety comes from the solvent (Table 1). All of the products were characterized by <sup>1</sup>H and <sup>13</sup>C NMR spectroscopy and mass spectrometric analysis.

The reaction of compound **4** with K<sub>2</sub>CO<sub>3</sub> in the presence of propargyl bromide under refluxing conditions in ethanol/water (4:1) afforded ethyl 5-(prop-2-yn-1-ylamino)-1-naphthoate (**5**) in good yield. Furthermore, as shown in Scheme 1, compound **5** underwent the [2 + 3] cycloaddition reaction with azidomethylferrocene to afford compound **6** in 75% yield. Interestingly, the presence of 1,8-diazabicyclo[5.4.0]undec-7-ene (DBU), a non-nucleophilic base, in the reaction mixture helps the deprotonation of the amine to obtain the imine,

which acts a linker between the triazole unit and the naphtholate moiety. Compound **6** was fully characterized by <sup>1</sup>H and <sup>13</sup>C NMR spectroscopy, electrospray ionization mass spectrometry (ESI-MS), and elemental analysis. Additionally, the molecular structure of compound **6** was unambiguously established by single-crystal X-ray diffraction analysis. After successfully synthesizing complex **6**, we wondered whether the metal-complexation-inhibited C=N isomerization-induced quenching mechanism could be used in the design of a fluorescence turn-on probe for metal ions. With this idea in mind, we investigated the sensing ability of **6** toward various metal cations. Excellent sensitivity and selectivity as well as a huge turn-on fluorescence response toward Hg<sup>2+</sup> and H<sup>+</sup> ions in CH<sub>3</sub>CN/H<sub>2</sub>O solution (2:8 v/v) were exhibited by the system. The host–guest complexation properties of receptor **6** were systematically investigated by UV–vis and fluorescence spectroscopy, electrochemistry, and <sup>1</sup>H NMR spectroscopic titration along with computational studies.

**X-ray Structure Analysis of Compound 6.** The single-crystal X-ray analysis showed that compound **6** crystallized in the monoclinic noncentrosymmetric system with space group *P*2<sub>1</sub>/*c* (Figure 1). All of the bond distances, including the C–N bond in the five-membered triazole ring (avg ~1.331 Å), are in the normal ranges and that the C14–N1 bond is little shorter because of the presence of a double bond (Figure 1).

**UV–Vis Absorption Studies.** The UV–vis binding interaction studies of receptor **6** in CH<sub>3</sub>CN/H<sub>2</sub>O (10<sup>−4</sup> M) against Li<sup>+</sup>, Na<sup>+</sup>, K<sup>+</sup>, Ag<sup>+</sup>, Ca<sup>2+</sup>, Mg<sup>2+</sup>, Mn<sup>2+</sup>, Fe<sup>2+</sup>, Al<sup>3+</sup>, Cr<sup>3+</sup>, Co<sup>2+</sup>, Cu<sup>2+</sup>, Zn<sup>2+</sup>, Cd<sup>2+</sup>, Ni<sup>2+</sup>, Hg<sup>2+</sup>, and Pb<sup>2+</sup> cations (as their perchlorate salts) showed a selective response to the Hg<sup>2+</sup> ion.

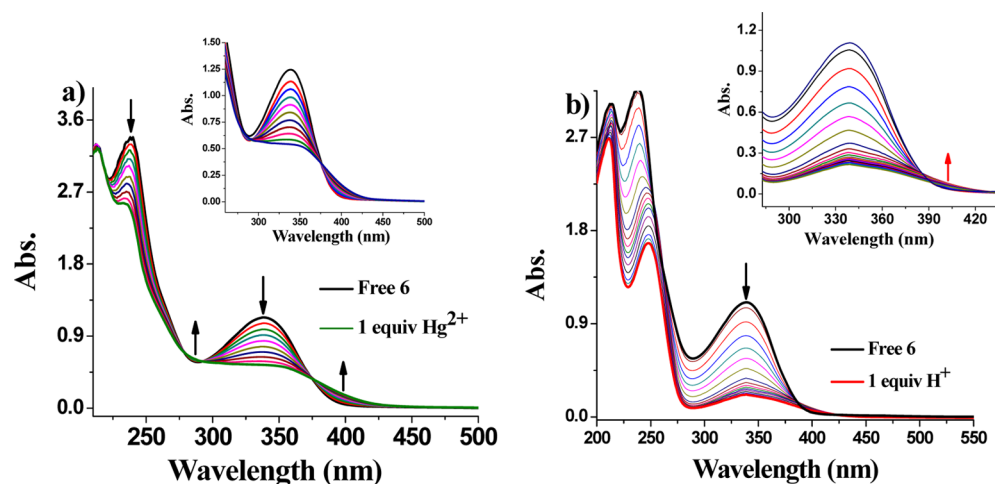
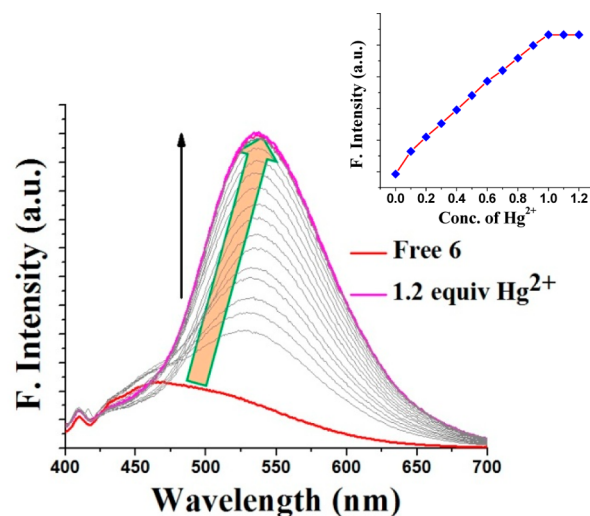


**Figure 2.** Changes in the absorption spectra of **6** in  $\text{CH}_3\text{CN}/\text{H}_2\text{O}$  ( $10^{-5}$  M) upon addition of increasing amounts of (a)  $\text{Hg}^{2+}$  and (b)  $\text{H}^+$  ions up to 1 equiv. The insets show expanded region.

The solutions of different cations were added separately to the prepared solution of compound **6**, and UV–vis absorption spectra were recorded. Except for  $\text{Hg}^{2+}$  ion, no metal ion exhibited any kind of significant effect on the absorption spectrum (Figure S15). Addition of a low concentration of  $\text{Hg}^{2+}$  led to a significant change in the UV–vis spectrum. To gain insight, an absorption titration of receptor **6** was performed with  $\text{Hg}^{2+}$  ion. The titration experiment was accomplished through stepwise addition of a solution of the metal salt ( $c = 10^{-5}$  M) to a solution of receptor **6** ( $c = 10^{-5}$  M). The UV–vis spectrum of receptor **6** shows a high-energy absorption band with a maximum at  $\lambda_{\text{max}} \sim 239$  nm (which may be due to a  $\pi-\pi^*$  excitation) and a low-energy absorption band at  $\lambda_{\text{max}} \sim 338$  nm. The UV–vis absorption spectrum of receptor **6** was found to be perturbed significantly upon the gradual addition of  $\text{Hg}^{2+}$  ion (Figure 2a). After the addition of 1 equiv of  $\text{Hg}^{2+}$  to **6**, the absorption bands at around 239 nm ( $33\,898\text{ M}^{-1}\text{cm}^{-1}$ ) and 338 nm ( $11\,461\text{ M}^{-1}\text{cm}^{-1}$ ) were decreased with the concomitant appearance of new low-energy band at 397 nm ( $530\text{ M}^{-1}\text{cm}^{-1}$ ). Two well-defined isosbestic points were found at ca. 292 and 375 nm, indicating that a net interconversion between the uncomplexed and complexed species occurs. In addition to the  $\text{Hg}^{2+}$  ion, the stepwise addition of  $\text{H}^+$  ion led to significant changes in the UV–vis absorption spectrum of compound **6** (Figure 2b). After the addition of 1 equiv of  $\text{H}^+$  to **6**, the absorption bands at around 239 and 338 nm were decreased simultaneously along with the appearance of a new weak peak at 401 nm. The stoichiometry of the complex formed between the ligand and  $\text{Hg}^{2+}$  is 1:1 as determined from the Job's plot (Figure S16). This result was also supported by ESI-MS, where a peak at  $m/z$  792 corresponds to the 1:1 complex of **6** with  $\text{Hg}^{2+}$  ion (Figure S17). Furthermore, the formation of a 1:1 complex of **6** with  $\text{Hg}^{2+}$  ion was confirmed by elemental analysis of the isolated [**6**· $\text{Hg}^{2+}$ ] species.

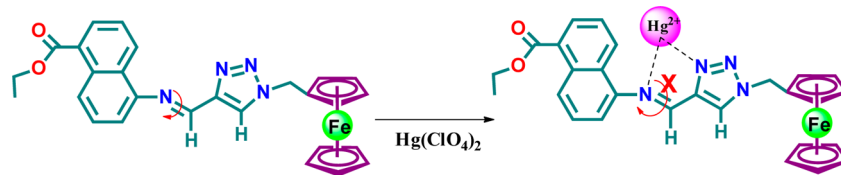
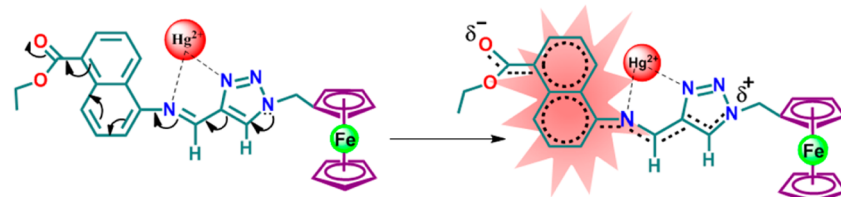
**Fluorescence Studies.** The photophysical properties of compound **6** were investigated by fluorescence spectroscopy measurements. Upon addition of 1 equiv of  $\text{Li}^+$ ,  $\text{Na}^+$ ,  $\text{K}^+$ ,  $\text{Ag}^+$ ,  $\text{Ca}^{2+}$ ,  $\text{Mg}^{2+}$ ,  $\text{Mn}^{2+}$ ,  $\text{Fe}^{2+}$ ,  $\text{Cr}^{3+}$ ,  $\text{Al}^{3+}$ ,  $\text{Co}^{2+}$ ,  $\text{Cu}^{2+}$ ,  $\text{Zn}^{2+}$ ,  $\text{Cd}^{2+}$ ,  $\text{Ni}^{2+}$ , and  $\text{Pb}^{2+}$  ions to a  $\text{CH}_3\text{CN}/\text{H}_2\text{O}$  (2:8 v/v) solution of compound **6**, no changes in the fluorescence spectrum were observed except in the case of  $\text{Hg}^{2+}$  ion (Figure S18). Surprisingly, addition of  $\text{Hg}^{2+}$  ion showed a remarkable

enhancement of the fluorescence with a large bathochromic shift in the emission wavelength from 468 to 536 nm ( $\Delta\lambda = 68$  nm). In order to study the sensitivity of receptor **6** toward  $\text{Hg}^{2+}$  ion, a fluorescence titration experiment was carried out. As shown in Figure 3, compound **6** exhibits weak fluorescence ( $\phi$



**Figure 3.** Fluorescence emission titration of compound **6** ( $10^{-8}$  M) upon addition of  $\text{Hg}^{2+}$  ion up to 1 equiv in  $\text{CH}_3\text{CN}/\text{H}_2\text{O}$  (2:8 v/v) solution.

$= 0.009$ )<sup>33</sup> at 468 nm when excited at 365 nm in  $\text{CH}_3\text{CN}/\text{H}_2\text{O}$  (2:8 v/v) solution. The weakly fluorescent nature of compound **6** is mainly due to the  $\text{C}=\text{N}$  bond isomerization-induced quenching effect. However, upon addition of  $\text{Hg}^{2+}$  ion, the fluorescence intensity remarkably increased and became nearly constant once the amount of  $\text{Hg}^{2+}$  reached 1 equiv. As a result, an approximately 58-fold enhancement of the fluorescence quantum yield was observed ( $\phi = 0.52$  for **6**). The huge fluorescence enhancement of **6** upon addition of  $\text{Hg}^{2+}$  strongly suggests that the  $\text{C}=\text{N}$  isomerization-induced quenching is inhibited in the [**6**· $\text{Hg}^{2+}$ ] adduct as a result of the formation of a rigid five-membered ring that prevents the  $\text{C}=\text{N}$  bond isomerization (Scheme 3). The selective fluorescence enhancement of  $\text{Hg}^{2+}$  could be due to more effective coordination of  $\text{Hg}^{2+}$  with the nitrogen atom of the  $\text{C}=\text{N}$  bond and the

Scheme 3. Proposed Mode of Interaction between Receptor 6 and Hg<sup>2+</sup>Scheme 4. Schematic Representation of Fluorescence Turn-On upon Hg<sup>2+</sup> Coordination

nitrogen atom of the triazole ring of compound **6** in comparison with other metal ions.

The energy of the ICT state can be regulated by varying the strengths of the donor and acceptor groups, which are distinctive of an ICT chromophore.<sup>34–36</sup> Increasing the strength of the donor group and extending the conjugation in the molecule lead to an enhancement of the charge separation and dipole moment. Consequently, the energy of the ICT state decreases. Spectroscopically, this is evident from a red shift of the UV–vis and fluorescence emission spectra.<sup>37</sup> Addition of Hg<sup>2+</sup> ion makes the molecule rigid through the formation of a five-membered ring, and as a result, electron delocalization from the N atom of the triazole ring (donor) to the ester moiety (acceptor) is much more viable (Scheme 4). Consequently, an enhancement of dipole moment and charge separation takes place, thereby leading to a large red shift of 68 nm in the fluorescence emission spectrum.

In order to determine the sensitivity of receptor **6**, a fluorescence titration of **6** ( $9 \times 10^{-8}$  M) with Hg<sup>2+</sup> ( $9 \times 10^{-8}$  M) in CH<sub>3</sub>CN/H<sub>2</sub>O (2:8 v/v) was performed. No detectable change was observed in the fluorescence spectrum up to an analyte concentration of 0.02 equiv of Hg<sup>2+</sup>. In the presence of 0.03 equiv of Hg<sup>2+</sup>, an appreciable enhancement with a red shift in the signal intensity was observed, whereas the maximum fluorescence intensity was observed in the presence of 1 equiv of Hg<sup>2+</sup> ion. This experiment shows that the low detection limit (DL) of **6** is  $2.7 \times 10^{-9}$  M (2.7 ppb) for Hg<sup>2+</sup>. Alternatively, to evaluate limit of detection (LOD), we fitted a straight line (data extracted from Figure 3) and applied the extensively used criterion  $\text{LOD} = 3.3\sigma/S$ , where  $\sigma$  is the standard deviation of the blank and  $S$  is the slope of the calibration curve. The detection limit (taken as  $3.3\sigma/S$ ) is in the same range as obtained from other methods also. The quantification limit (LOQ) for probe **6** (taken as  $10\sigma/S$ ) is 8.1 nM for Hg<sup>2+</sup> ion. The value of the binding constant of Hg<sup>2+</sup> with **6** was determined from the emission intensity data following the modified Benesi–Hildebrand equation:<sup>38,39</sup>  $1/\Delta I = 1/\Delta I_{\text{max}} + (1/K[\text{Hg}^{2+}])(1/\Delta I_{\text{max}})$ , where  $\Delta I = I - I_0$  and  $\Delta I_{\text{max}} = I_{\text{max}} - I_0$ , in which  $I$ ,  $I_{\text{max}}$  and  $I_0$  are the emission intensities of **6** considered at an intermediate Hg<sup>2+</sup> concentration, in the absence of Hg<sup>2+</sup>, and at a concentration of complete interaction, respectively, and  $K$  is the binding constant, and  $[\text{Hg}^{2+}]$  is the Hg<sup>2+</sup> concentration. From the plot of  $\Delta I_{\text{max}}/\Delta I$

against  $[\text{Hg}^{2+}]^{-1}$ , the value of  $K$  (15%) extracted from the slope was  $7.2 \times 10^7 \text{ M}^{-1}$  for **6** with Hg<sup>2+</sup> (Figure S19).

Furthermore, in order to obtain the optimal experimental conditions and acquire a high signal-to-noise ratio for detection of Hg<sup>2+</sup>, the incubation time was investigated. For this experiment, the net signal  $\Delta F = F - F_0$  was used as the standard, where  $F$  and  $F_0$  are the fluorescence intensities in the presence and absence of the target Hg<sup>2+</sup>, respectively. Moreover, the incubation time of Hg<sup>2+</sup> can affect the signal amplification strongly. As shown in the inset of Figure 3, with increasing Hg<sup>2+</sup> concentration the fluorescence difference increased rapidly and then attained saturation after addition of 1 equiv. Therefore, 1 equiv of Hg<sup>2+</sup> was found to be optimum and was selected for further experiment. To accomplish the optimum conditions for binding, the effect of the incubation time for Hg<sup>2+</sup> was also investigated. As indicated in Figure 4, the fluorescence intensity difference increased

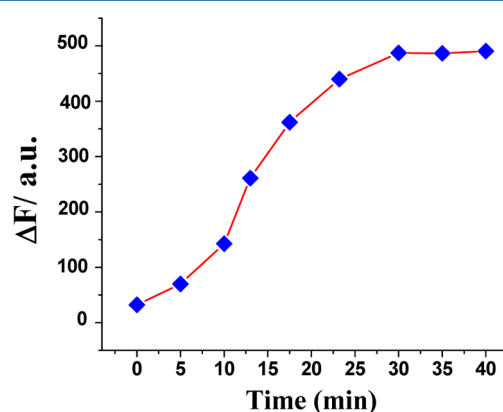
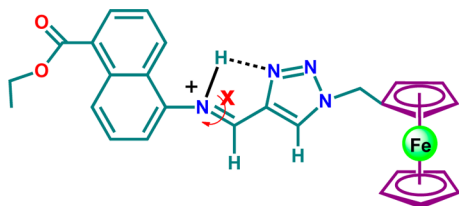


Figure 4. Optimization of the incubation time for Hg<sup>2+</sup> ion.

simultaneously with the interval of 5 min and it reached the highest  $\Delta F$  value at 30 min. Upon further prolongation of the incubation time, the fluorescence intensity difference was saturated, which may be the result of complete complexation of Hg<sup>2+</sup> with probe **6**. Hence, an incubation time of 30 min was selected for the optimization conditions.

Furthermore, we wondered whether the fluorescence emission of probe **6** could be regulated through inhibition of the C=N isomerization-induced quenching process by an intramolecular hydrogen bond. Natural bond orbital (NBO)

charge analysis using density functional theory (DFT) calculations revealed that the imine nitrogen ( $-\text{CH}=\text{N}$ ) accumulated more charge, as can be seen from its natural valence population of +5.44, compared with the three nitrogen atoms of the triazole ring. Therefore, addition of acid can protonate the imine N to form the iminium ion. The iminium hydrogen atom can form a strong hydrogen bond with one of the N atoms of the triazole ring ( $\text{N}_{\text{triaz}} \cdots \text{H}$  distance = 2.307 Å by DFT calculations), resulting the formation of a five-membered heterocyclic ring (Figure 5).<sup>40</sup> As a result of this attractive



**Figure 5.** Formation of a five-membered heterocyclic ring upon protonation of ligand 6.

hydrogen-bond-inhibited  $\text{C}=\text{N}$  isomerization, probe 6 shows a drastic (20-fold) enhancement of the fluorescence emission upon addition of acid (Figure 6a). The reversibility of this process (deprotonation) was investigated by adding sodium hydroxide as a base. As shown in Figure 6b, upon addition of NaOH up to 1 equiv with respect to the protonated solution, the fluorescence steadily decreases. This experiment clearly indicates that  $\text{H}^+$  and  $\text{OH}^-$  can be used to regulate the off–on–off fluorescence switching of molecule 6. Thus, this concept could be further utilized to construct a molecular logic gate.

**Construction of the Logic Gate.** Inspired by the observations of the sensing capabilities of fluorescence of probe 6 toward  $\text{Hg}^{2+}$ ,  $\text{H}^+$ , and  $\text{OH}^-$ , we developed a fluorometric logic system capable of performing individual logic operations. The presence and absence of each of these inputs were coded with Boolean logic functions as 1 and 0, respectively. The enhanced and quenched fluorescence output values (at 536 nm) were assigned as “1” (the on state, above the threshold value) and “0” (the off state, below the threshold value), respectively. The output value was defined as 1 when the relative fluorescence intensity was higher than 25 and 0 when the relative intensity was lower than 25. The fluorescence response of receptor 6 exhibits INHIBIT and OR logic gates,

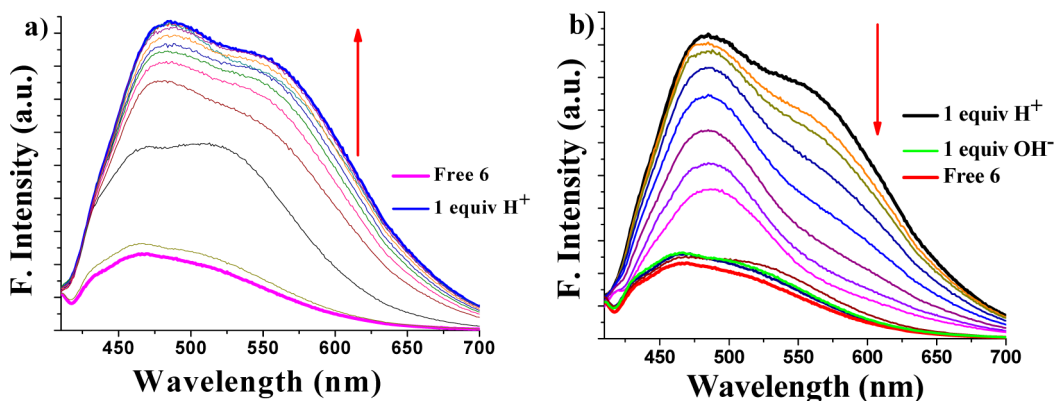


**Figure 6.** (a) Fluorescence titration of compound 6 upon addition of  $\text{H}^+$  ion up to 1 equiv in  $\text{CH}_3\text{CN}/\text{H}_2\text{O}$  solution. (b) Fluorescence spectra of 6 upon the addition of 1 equiv of  $\text{OH}^-$  in the presence of 1 equiv of  $\text{H}^+$ .

and the circuits are shown in Figure 7. The values of  $I/I_0$  at 536 nm for 6 with different combinations of varying concentrations

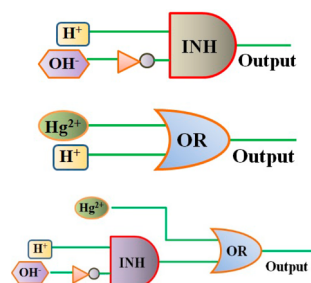


**Figure 7.** Circuits for different logic gates.

of  $\text{H}^+$  and  $\text{OH}^-$  correspond to an INHIBIT logic gate. A binary INHIBIT logic operation, which is represented by the situation in which the output is 1 only if one particular input is present and the other is absent, can be implemented as a gate with  $\text{H}^+$  and  $\text{OH}^-$  as double inputs (Figure 7). As shown in Figure 7, an OR logic gate was designed using  $\text{Hg}^{2+}$  and  $\text{H}^+$  ions as inputs. After the successful generation of the basic binary logic gates, it was reasonable to make an attempt to construct some integrated gates as well. With this idea in mind, a three-input INHIBIT–OR combinational gate was generated, where  $\text{H}^+$  and  $\text{OH}^-$  constituted the inputs of an INHIBIT gate, whose output was cascaded along with  $\text{Hg}^{2+}$  into an OR gate.

Four different conditions were investigated (Figure 8A):  $\text{H}^+$  as input 1 at 0 mM (low, 0, bars a and c) or 15 mM (high, 1, bars b and d) and  $\text{OH}^-$  as input 2 at 0 mM (low, 0, bars a and b) or 15 mM (high, 1, bars c and d). As shown in Figure 8A, the output value of  $I/I_0$  at 536 nm has a maximum ( $I/I_0 = 88$ ) in the presence of only  $\text{H}^+$ . On the other hand, the value of  $I/I_0$  is at a low level ( $I/I_0 < 25$ ) for any other combination. This behavior is well-consistent with an INHIBIT logic gate. Analogously, the different input combinations of  $\text{Hg}^{2+}$  and  $\text{H}^+$  for 6 can behave like an OR logic gate with the value of  $I/I_0$  (536 nm) as the output (Figure 8B). In this OR logic gate,  $\text{Hg}^{2+}$  and  $\text{H}^+$  have been taken as inputs 1 and 2, respectively, with 15 mM concentration. On combination of the three inputs  $\text{Hg}^{2+}$ ,  $\text{H}^+$ , and  $\text{OH}^-$  a combinational INHIBIT–OR logic circuit can be made (Figure 8C): out of eight possible input combinations, the output value of  $I/I_0$  at 536 nm is high when

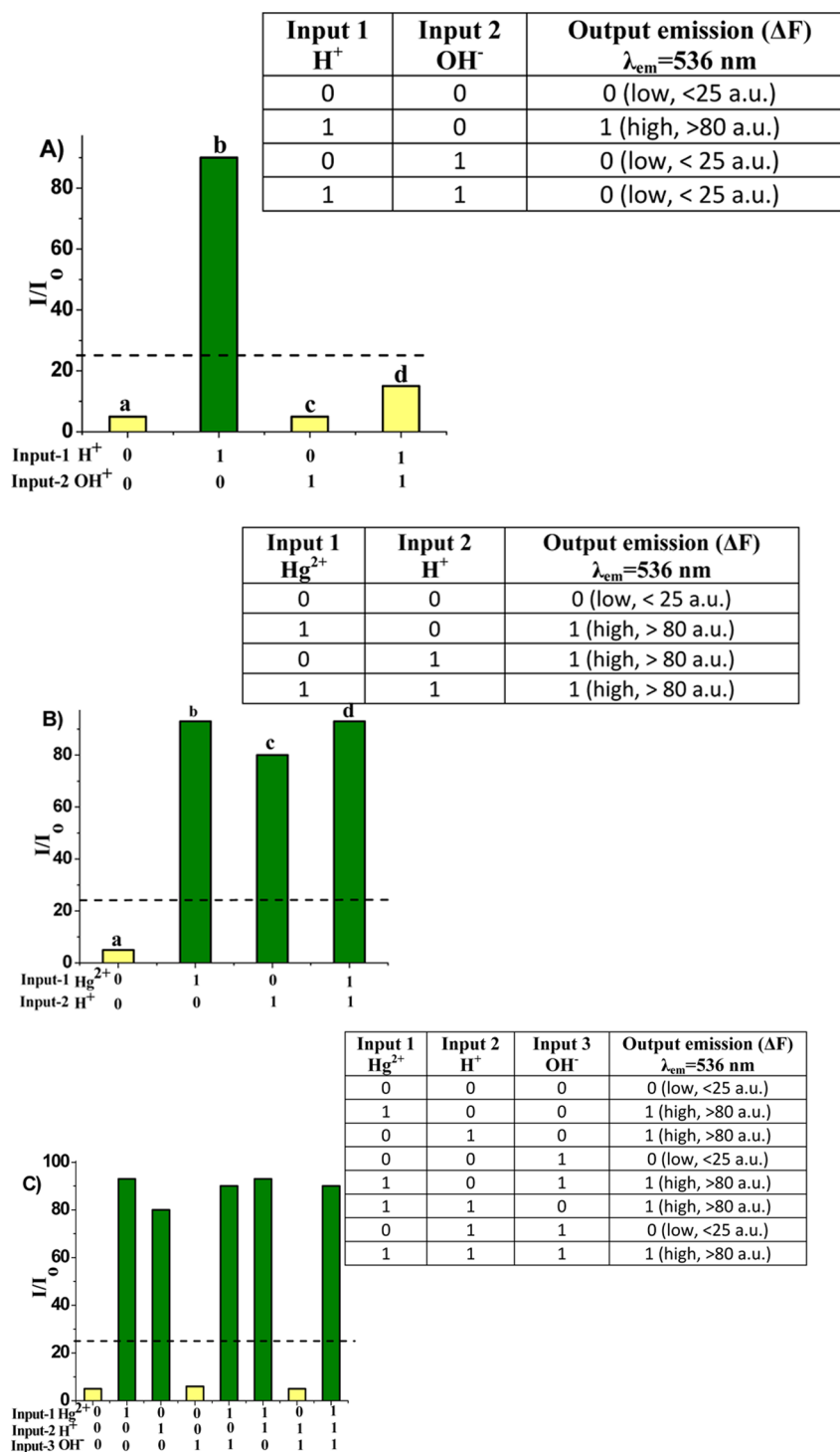


**Figure 8.** (A) INHIBIT logic gate constructed with  $H^+$  and  $OH^-$  as an input and (B) OR logic gate constructed with  $Hg^{2+}$  and  $OH^-$  at  $I/I_0 = 536$  nm. (C) Combinational logic operation.

$Hg^{2+}$  and  $H^+$  are present. The threshold for all of the logic operations was set at 25.

**Effect of pH.** To elucidate the role of pH in the detection of  $Hg^{2+}$  ion, the pH titration was carried out with free **6** and in the presence of 1.0 equiv of  $Hg^{2+}$  ion in  $CH_3CN/H_2O$  (2:8 v/v) solution. The pH of the free ligand was found to be 6.8. In the pH range from 2 to 4.5, a drastic increase in fluorescence intensity (Figure 9) with a red shift of 18 nm was observed for free **6**, whereas no significant change in fluorescence intensity was observed for the  $[6 \cdot Hg^{2+}]$  adduct (Figure S20a). Similarly,

no significant change in fluorescence intensity was exhibited when  $Hg^{2+}$  ion was added to the protonated solution of free **6** (pH range 2–4.5) (Figure S20b). From these experiments it is evident that no interaction would be possible between **6** and  $Hg^{2+}$  ion at acidic pH because of the electric charge repulsion between protonated imine (the imine was protonated in this acidic solution) and  $Hg^{2+}$  ion. In a similar fashion,  $H^+$  ion also cannot perturb the fluorescence spectrum of the  $[6 \cdot Hg^{2+}]$  adduct because the imine N atom is no longer available to be protonated once it coordinates with  $Hg^{2+}$ .

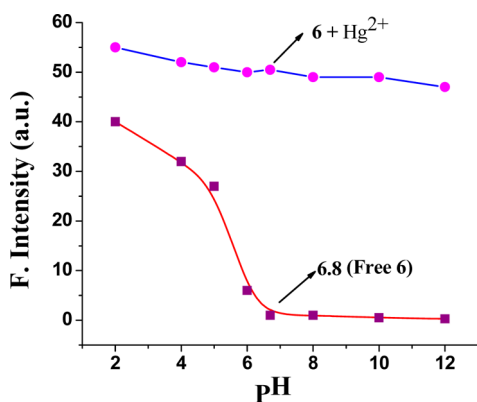


**Figure 9.** Influence of pH on the fluorescence emission of **6** and the [**6**·Hg<sup>2+</sup>] complex.

With the increase of pH from 6.0 to 12, no significant changes in fluorescence intensity were observed for free ligand **6**. Similar results were obtained when the fluorescence was measured in the presence of 1 equiv of Hg<sup>2+</sup> ion in the pH range of 6–12. These results suggested that the [**6**·Hg<sup>2+</sup>] adduct was stable enough under strongly basic conditions (pH ~ 12) that the OH<sup>−</sup> could not displace the receptor to form Hg(OH)<sub>2</sub>. To the best of our knowledge, this is the first ferrocene-based electrochemical and fluorescent chemosensor for Hg<sup>2+</sup> ion working over such a broad pH range from 6 to 12.

**Electrochemical Study.** The metal recognition properties of compound **6** were investigated by an electrochemical (cyclic voltammetry) study. The electrochemical behavior was investigated in the presence of several metal cations, such as Li<sup>+</sup>, Na<sup>+</sup>, K<sup>+</sup>, Ag<sup>+</sup>, Ca<sup>2+</sup>, Mg<sup>2+</sup>, Cr<sup>3+</sup>, Al<sup>3+</sup>, Zn<sup>2+</sup>, Fe<sup>3+</sup>, Ni<sup>2+</sup>, Co<sup>2+</sup>, Cu<sup>2+</sup>, Cd<sup>2+</sup>, Hg<sup>2+</sup>, and Pb<sup>2+</sup> (as their perchlorate salts), in a CH<sub>3</sub>CN/H<sub>2</sub>O (2:8 v/v) solution of **6** containing 0.1 M [(*n*-Bu)<sub>4</sub>N]ClO<sub>4</sub> as the supporting electrolyte. The free receptor **6** displayed a reversible one-electron redox potential at the half-wave potential value  $E_{1/2} = 0.584$  V versus the ferrocene/ferrocenium redox couple (Fc/Fc<sup>+</sup>). No perturbation of the cyclic voltammogram (CV) of **6** was observed except in the case of Hg<sup>2+</sup> ion (Figure S21). As shown in Figure 10, stepwise addition of Hg<sup>2+</sup> up to 1 equiv induced a significant anodic shift of  $\Delta E_{1/2} = 72$  mV for **6** due to the formation of a new complex species.

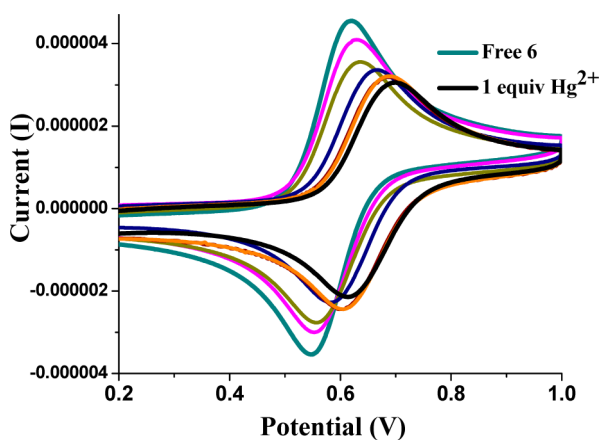


**Figure 10.** Evolution of the CV of **6** (10<sup>−4</sup> M) in CH<sub>3</sub>CN/H<sub>2</sub>O (2:8 v/v) using [(*n*-Bu)<sub>4</sub>N]ClO<sub>4</sub> as the supporting electrolyte as 1 equiv of Hg<sup>2+</sup> was added. The scan rate was 0.05 V s<sup>−1</sup>.

**Visual Detection of Hg<sup>2+</sup>.** In colorimetric experiments, significant color changes of a CH<sub>3</sub>CN/H<sub>2</sub>O (2:8 v/v) solution of **6** were observed upon addition of Hg<sup>2+</sup> ion over the other tested metal cations (Figure 11). A distinct color change of

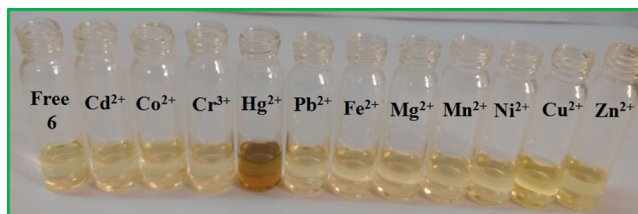


**Figure 11.** Visual color changes observed for **6** (10<sup>−3</sup> M) in CH<sub>3</sub>CN/H<sub>2</sub>O after addition of 1 equiv of several metal cations.

receptor **6** from faint yellow to pale orange was observed in the presence of Hg<sup>2+</sup> ion, which indicates the sensitive and selective “naked eye” detecting ability of **6** for Hg<sup>2+</sup> ion. When 1 equiv of different metal cations (Li<sup>+</sup>, Na<sup>+</sup>, K<sup>+</sup>, Ag<sup>+</sup>, Ca<sup>2+</sup>, Mg<sup>2+</sup>, Mn<sup>2+</sup>, Al<sup>3+</sup>, Cr<sup>3+</sup>, Co<sup>2+</sup>, Cu<sup>2+</sup>, Zn<sup>2+</sup>, Cd<sup>2+</sup>, Ni<sup>2+</sup>, and Pb<sup>2+</sup>, as their perchlorate salts) was added to the solution of ligand **6** in CH<sub>3</sub>CN/H<sub>2</sub>O (2:8 v/v), no significant color changes were observed. Interestingly, Hg<sup>2+</sup> ion showed a significant color change even at very low concentration (10<sup>−5</sup> M) (Figure S22). Furthermore, to investigate the practical analytical applicability of probe **6**, we investigated the reversibility of **6** (Figure S23) and its action in a solid support (Figure S24).

**<sup>1</sup>H NMR Spectroscopic Titration.** In order to confirm the binding mode of the receptor with Hg<sup>2+</sup> ion, an <sup>1</sup>H NMR spectroscopic titration study was carried out in DMSO-*d*<sub>6</sub> (Figure 12). The extensive NMR spectroscopy characterization was undertaken to assign the two near-conjugated −CH protons. With the help of the two-dimensional <sup>1</sup>H–<sup>13</sup>C heteronuclear single-quantum coherence (HSQC) NMR spectroscopic method, the protons H<sub>a</sub> and H<sub>b</sub> were unambiguously assigned as the triazole −CH and the −N=CH protons, respectively (Figure S25). The ‘d’ carbon atom of the triazole ring is known to resonate at 122–124 ppm,<sup>41</sup> which is correlated with the proton at 8.85 ppm. Thus, on the basis of this correlation we assigned the peak at 8.85 ppm to the triazole −CH proton. Upon addition of Hg<sup>2+</sup> ion to a solution of receptor **6**, the following significant spectral changes were observed: (i) Proton H<sub>a</sub> attached to the triazole unit was downfield-shifted by 0.12 ppm and (ii) proton H<sub>b</sub> attached to the C=N bond was downfield-shifted by 0.15 ppm with increasing Hg<sup>2+</sup> concentration, along with a decrease in the peak intensity. A polar aprotic solvent like DMSO may form a strong hydrogen-bonding interaction with highly acidic hydrogen atom (H<sub>b</sub>) of the −N=CH group, which may lead to the decrease in the peak height. (iii) Similarly, proton H<sub>c</sub> attached to the NCH<sub>2</sub> group was very slightly downfield-shifted by 0.05 ppm. No change in the chemical shifts were observed for other protons attached to the naphthalene moiety and ester unit. From the <sup>1</sup>H NMR chemical shifts, it is evident that the probable binding mode of the Hg<sup>2+</sup> ion is with the N atom of the C=N linkage and one of the N atoms of the triazole ring (the one closest to the imine N).

**Theoretical (DFT) Studies.** Quantum-chemical calculations were performed to reveal the structural and electronic parameters that control the aforementioned responses of receptor **6** toward Hg<sup>2+</sup>. The ligand-to-metal binding ratio of **6** and Hg<sup>2+</sup> was found to be 1:1 on the basis of spectral data

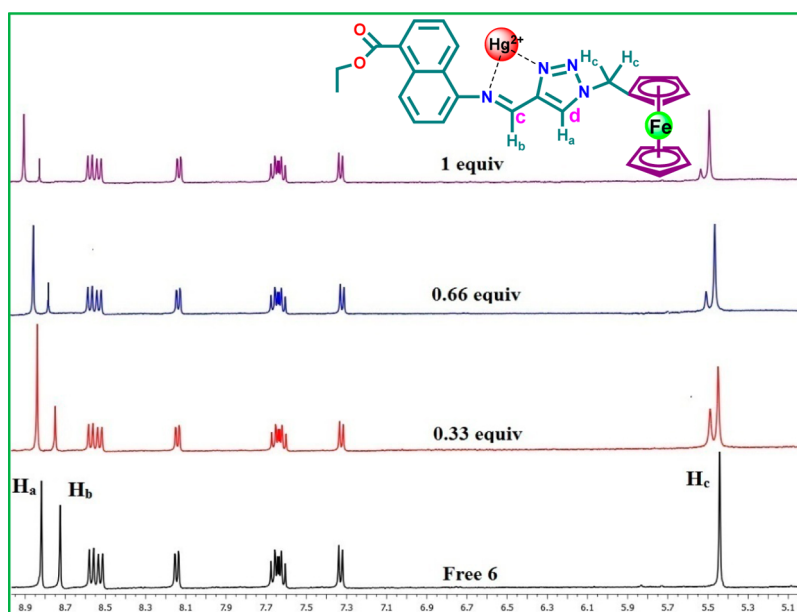


Figure 12. Proposed mode of binding between receptor **6** and  $\text{Hg}^{2+}$  in  $\text{DMSO}-d_6$ .

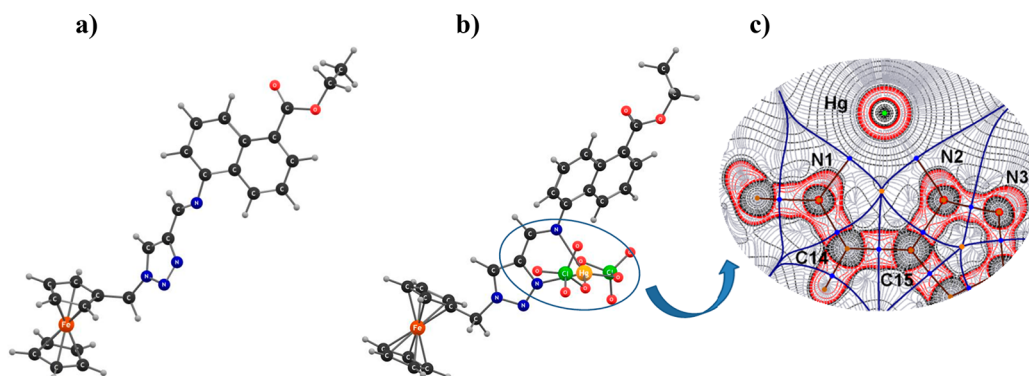


Figure 13. Optimized geometries of (a) free **6** and (b)  $[\mathbf{6}\cdot\text{Hg}^{2+}](\text{ClO}_4)_2$ . (c) Contour line diagram of the Laplacian of the electron density,  $\nabla^2\rho(r)$ , of the complex in the  $\text{N}2\text{--N}1\text{--Hg}$  plane. Solid red lines indicate areas of charge concentration ( $\nabla^2\rho(r) < 0$ ), while dashed black lines show areas of charge depletion ( $\nabla^2\rho(r) > 0$ ). Solid brown lines connecting the atomic nuclei are the bond paths. The thick blue lines separating the atomic basins indicate the zero-flux surfaces crossing the molecular plane. Blue, orange, and green dots indicate bond critical points, ring critical points, and cage critical point, respectively.

(e.g., absorption and emission spectra) as well as electrochemical and ESI-MS data. Furthermore, the formation of the mononuclear complex  $[\mathbf{6}\cdot\text{Hg}^{2+}](\text{ClO}_4)_2$  was modeled by DFT calculations at the B3LYP level using the Gaussian 09 package, as explained in [Computational Details](#). The corresponding optimized structures are shown in [Figure 13](#).

The geometry optimization of  $[\mathbf{6}\cdot\text{Hg}^{2+}](\text{ClO}_4)_2$  at the B3LYP/def2-SVP level of theory resulted in a slight conformational change of the free ligand. The  $\text{--CH}_2\text{--N}$  (triazole) bond is rotated in such a way that both the imine N and one of the triazole N atoms can come close to form a binding core for the  $\text{Hg}^{2+}$  ion. In this binding situation, Hg exhibits a distorted tetrahedral  $\text{N}_2\text{Cl}_2$  coordination. The  $\text{Hg}^{2+}$  center shows a distorted geometry that deviates from both the square-planar and tetrahedral geometries. Among the four coordinates, both of the  $\text{Hg--N}$  bonds ( $d_{\text{Hg--N}1} = 2.476 \text{ \AA}$  and  $d_{\text{Hg--N}2} = 2.390 \text{ \AA}$  in  $[\mathbf{6}\cdot\text{Hg}^{2+}](\text{ClO}_4)_2$ ) are relatively weak, as evidenced by the low Wiberg bond index values ( $\text{WBI}_{\text{Hg--N}1} = 0.2236$  and  $\text{WBI}_{\text{Hg--N}2} = 0.2223$  in  $[\mathbf{6}\cdot\text{Hg}^{2+}](\text{ClO}_4)_2$ ), whereas the other two sites are occupied by two Cl atoms of the  $\text{ClO}_4$  units.

To analyze the nature of the bonding, we examined the plot of the Laplacian of the electron density,  $\nabla^2\rho(r)$ , of **6** ([Figure 13c](#)). The figure shows that the  $\text{N--Hg}$  bond in **6** has an area of charge concentration ( $\Delta^2\rho(r) < 0$ , solid red lines) at N while the Hg end carries a charge depletion area ( $\Delta^2\rho(r) > 0$ , solid lines), indicating the existence of an electrostatic interaction between the N and Hg centers. The evidence of this interaction can also be verified by the presence of a large electron density over the Hg-centered LUMO ([Figure S26](#)) due to electron delocalization from the N atom. The bond between N and Hg is relatively weak, as is evident from the electron density values ([Table S1](#)) at the  $\text{N}1\text{--Hg}/\text{N}2\text{--Hg}$  bond critical points. Furthermore, the ring critical point of the  $\text{N}1\text{--C}14\text{--C}15\text{--N}2\text{--Hg}$  five-membered metallacycle ring shows a slight electron density (0.015 a.u.), which is in the favor of the formation of the five-membered metallacycle ring. Interestingly, our attempts to optimize the Hg complex with the cis isomer ([Figure S27](#)) led to an optimized geometry ([Figure S28](#)) that was 29.21 kJ/mol higher in energy compared with the Hg complex with the trans isomer. This indicates that upon

complexation with  $\text{Hg}^{2+}$  ion only one isomer (trans) get stabilized and no cis–trans isomerization of  $\text{C}=\text{N}$  is possible, thereby leading to a large fluorescence enhancement.

Frontier molecular orbitals (MOs) of **6** and its Hg complex  $[\text{6}\cdot\text{Hg}^{2+}](\text{ClO}_4)_2$  are shown in Figure 14 (and Figures S29 and

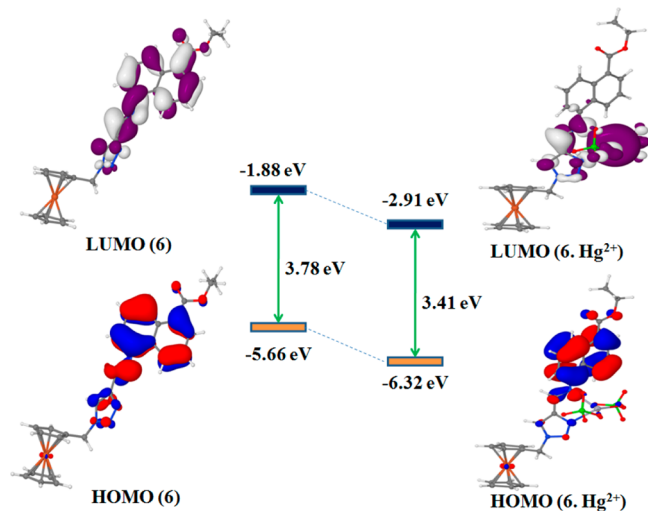


**Figure 14.** Frontier molecular orbitals (isovalue = 0.03) of (left) **6** and (right)  $[\text{6}\cdot\text{Hg}^{2+}](\text{ClO}_4)_2$  as obtained from DFT calculations.

S30). In **6**, both the HOMO and LUMO were found to be majorly localized on the naphthalene unit (the  $\pi$  and  $\pi^*$  orbitals, respectively). In  $[\text{6}\cdot\text{Hg}^{2+}](\text{ClO}_4)_2$ , the HOMO is virtually same as that of the free ligand, but the LUMO is majorly found in the binding core, which is essentially a Hg-based vacant orbital. Therefore, the computational studies and Laplacian electron density plot as well as MO analysis support our proposed binding mode of ligand **6** with  $\text{Hg}^{2+}$  ion.

Furthermore, time-dependent DFT (TD-DFT) calculations were performed to obtain detailed information about the absorption of **6** and  $[\text{6}\cdot\text{Hg}^{2+}](\text{ClO}_4)_2$  in  $\text{CH}_3\text{CN}$  as a solvent. The TD-DFT calculations showed two absorption maxima at 227 and 335 nm for **6** which nicely corroborate the experimental values (238 and 339 nm). The higher-energy peak is majorly due to the electronic transition from the HOMO (naphthalene-based  $\pi$  orbitals) to the LUMO+2, which is largely localized on ferrocene with a slight contribution from the triazole ligand. The lower-energy peak is due to the transition from the naphthalene-based HOMO to the LUMO, which are essentially  $\pi$  and  $\pi^*$  orbitals, respectively. The UV–vis study showed decreased intensity of both absorption maxima upon binding with  $\text{Hg}^{2+}$  along with the appearance of a new low-energy peak. The TDDFT results indicate that the decrease in intensity is due to the less favored transition of the ferrocene lone pair (HOMO–2) to a vacant Hg orbital (LUMO). Furthermore, the DFT calculations show that the HOMO–LUMO gap diminishes upon complex formation (Figure 14), which satisfactorily corroborates the observed red shift in UV–vis study.

In addition, the geometry of the protonated species was optimized using DFT calculations at the B3LYP level, and the frontier MOs were also calculated (Figure S31). From the DFT-optimized geometry it is evident that after protonation, the iminium hydrogen atom can form a stable five-membered ring via a hydrogen-bonding interaction (2.307 Å) with the nearest N atom of the triazole ring (Figure S32). Furthermore,

TD-DFT calculations of the protonated ligand revealed that the UV–vis spectrum follows a trend similar to that of the  $\text{Hg}^{2+}$  complex. The low-energy band at  $\sim 257$  nm is responsible for a HOMO–9 to LUMO transition with a  $\sim 65\%$  contribution (the HOMO–9 is mainly based on  $\pi$  orbitals of the naphthalene unit, whereas the LUMO is based on the  $\pi^*$  orbitals with a major contribution from the triazole and imine units). The signal at  $\sim 365$  nm is majorly due to the HOMO–2 to LUMO transition with a  $\sim 90\%$  contribution (HOMO–2 is the ferrocene-based filled lone-pair orbitals) (Table S2).

The electrostatic potential surface (EPS) diagrams of the ligand and  $[\text{6}\cdot\text{Hg}^{2+}]$  were also calculated (Figure S33). It is evident from the EPS diagram of the Hg complex that there is a depletion of charge at the N end and an accumulation of charge (apart from localized electrons on the Cl atoms) at the O end of the ester moiety. The second-order perturbation energy analysis obtained from the NBO analysis shows that delocalization of the lone pairs of electrons from N2 and N3 to the empty Hg orbital (34.4 and 34.8 kcal/mol) and delocalization of the lone pair of electrons on N4 toward the ester moiety (36 kcal/mol) are highly favorable. This supports our proposed mechanism described in Scheme 4 for the fluorescence enhancement along with a large red shift.

## CONCLUSION

An optoelectronic molecular device for selective and sensitive detection of  $\text{Hg}^{2+}$  ion has been synthesized. The probe shows a huge enhancement of emission intensity with a large bathochromic shift upon addition of  $\text{Hg}^{2+}$  ion. Furthermore, a similar trend was also observed in the fluorescence emission spectra when the probe was treated with a strong acid. The presence of  $\text{Hg}^{2+}$  and  $\text{H}^+$  causes the inhibition of cis–trans isomerization around  $\text{C}=\text{N}$  by forming a rigid five-membered metallacycle and hydrogen-bonded framework, respectively, thereby leading to a fluorescence enhancement of the system. To the best of our knowledge, molecule **6** is the first example of a triazole- and imine-conjugated ferrocene–naphtholate system where the fluorescence signal can be modulated by both metal complexation and protonation/deprotonation strategies. Thus,  $\text{H}^+$  and  $\text{OH}^-$  have been used to regulate the off–on–off fluorescence switching of molecule **6**. On the basis of the on–off switching of the fluorescence output mechanism, basic OR and INHIBIT binary logic gates were developed using the  $\text{Hg}^{2+}$  and  $\text{H}^+$  ions and the  $\text{H}^+$  and  $\text{OH}^-$  ions, respectively. These basic binary logic gates were further attached to form an INHIBIT–OR combinational gate, which could be utilized in multitasking of biosensing of dual targets. The constructed combinational INHIBIT–OR logic gate functions not only in organic solution but also via conjugation with silica gel as a solid support.

## EXPERIMENTAL SECTION

**Materials and Methods.** The perchlorate salts of  $\text{Li}^+$ ,  $\text{Na}^+$ ,  $\text{K}^+$ ,  $\text{Cu}^{2+}$ , and  $\text{Hg}^{2+}$  as well as DBU and CuI were procured from Sigma-Aldrich and used directly without further purification. The perchlorate salts of  $\text{Ag}^+$ ,  $\text{Cr}^{3+}$ ,  $\text{Ca}^{2+}$ ,  $\text{Mg}^{2+}$ ,  $\text{Al}^{3+}$ ,  $\text{Fe}^{2+}$ ,  $\text{Mn}^{2+}$ ,  $\text{Zn}^{2+}$ ,  $\text{Pb}^{2+}$ , and  $\text{Co}^{2+}$  were purchased from Alfa Aesar. Ferrocene,  $N,N,N',N'$ -tetramethylethylenediamine (TMEDA),  $\text{POCl}_3$ ,  $m$ -butyllithium (2.5 M in hexane),  $\text{NaN}_3$ ,  $\text{NaBH}_4$ ,  $\text{K}_2\text{CO}_3$ ,  $\text{Na}_2\text{Cr}_2\text{O}_7$ , propargyl bromide, and  $\text{SnCl}_2\cdot 2\text{H}_2\text{O}$  were purchased from local chemicals. DMF and acetonitrile (HPLC) were purchased from Thermo Fisher Scientific and freshly distilled prior to use. Chromatography was carried out using 100–200 mesh silica gel and basic alumina in a column of 2.5 cm diameter. All of the necessary solvents were dried by conventional methods and

distilled under an atmosphere of  $N_2$  before use. Azidomethylferrocene was synthesized as per the literature procedure.<sup>42,43</sup> The cyclic voltammetry study was performed using glassy carbon as the working electrode, platinum as the auxiliary electrode, and  $Ag/Ag^+$  as the reference electrode. The experiments were carried out with a  $10^{-4}$  M solution of the sample in  $CH_3CN/H_2O$  (2:8 v/v) containing 0.1 M [ $(n-Bu)_4NClO_4$ ] as the supporting electrolyte. The CVs were recorded at a scan rate of  $0.05 V s^{-1}$ . The working electrode was cleaned after each run. The UV-vis spectra were measured using  $CH_3CN/H_2O$  (2:8 v/v) solutions at  $c = 10^{-5}$  M and the fluorescence spectra were measured at  $c = 10^{-8}$  M, as stated in the corresponding figure captions.

**Instrumentation.** The  $^1H$  and  $^{13}C$  spectra were recorded on Bruker 400 MHz FT-NMR spectrometers using tetramethylsilane as an internal reference. The absorption spectra were recorded with a Shimadzu 2450 UV-vis spectrophotometer at room temperature. Fluorescence was recorded with a HORIBA Scientific Fluoromax-4 spectrophotometer. Cyclic voltammetry was performed on a CH Instruments S8/39 electrochemical workstation. ESI-MS measurements were carried out on PerkinElmer Flexar SQ 300 MS detector. A SYSTRONICS  $\mu$  pH system 361 with a glass electrode was used for pH detection. CHN analysis was performed on a vario EL elemental CHNS analyzer. Melting points were measured in a Labotech melting point apparatus.

**Caution!** Metal perchlorate salts are potentially explosive under certain conditions. All due precautions should be taken while handling perchlorate salts.

**Synthesis of Compound 4.** A stirred cloudy solution of compound 3 (0.240 g, 0.987 mmol) in ethanol (10 mL) was added dropwise to a solution of  $SnCl_4 \cdot 2H_2O$  (1.336 g, 5.922 mmol) in concentrated hydrochloric acid (2 mL) at room temperature. The reaction mixture was refluxed for 2 h and then cooled to room temperature, and an aqueous solution of  $Na_2CO_3$  (10%) was added to quench the reaction. The reaction mixture was diluted with ethyl acetate and washed several times with water and then brine. The combined organic layer was dried over anhydrous  $Na_2SO_4$  and then evaporated under reduced pressure. The crude residue was purified by column chromatography using basic alumina. Elution with EtOAc/hexane (3:7 v/v) yielded ethyl 5-amino-1-naphthoate (4) as a pale-yellow oil (0.142 g, 67%).

$^1H$  NMR ( $CDCl_3$ , 400 MHz):  $\delta$  8.29 (d, 1H,  $H_{naphthalene}$ ,  $J = 8.8$  Hz), 8.10 (d, 1H,  $H_{naphthalene}$ ,  $J = 6.8$  Hz), 8.0 (d, 1H,  $H_{naphthalene}$ ,  $J = 8.4$  Hz), 7.43–7.37 (m, 2H,  $H_{naphthalene}$ ), 6.80 (d, 1H,  $H_{naphthalene}$ ,  $J = 7.2$  Hz), 4.47 (q, 2H,  $OCH_2$ ), 4.16 (s, 2H,  $NH_2$ ), 1.45 (t, 3H,  $CH_3$ ,  $J = 7.2$  Hz).  $^{13}C$  NMR ( $CDCl_3$ , 100 MHz):  $\delta$  168.1, 142.5, 132.0, 129.6, 128.1, 125.6, 124.1, 123.2, 116.4, 110.2, 61.1, 14.3. ESI-MS,  $m/z$  (relative intensity): 216 ( $M^+ + 1$ ); Anal. Calcd for  $C_{13}H_{13}O_2N$ : C, 72.54; H, 6.09; N, 6.51. Found: C, 72.47; H, 6.18; N, 6.44.

**Synthesis of Compound 5.** Compound 4 (0.190 g, 0.883 mmol) was dissolved in a 4:1 mixture of ethanol and water, and the solution was stirred. Then  $K_2CO_3$  (0.971 mmol) and propargyl bromide (0.883 mmol) were added to the stirred solution, and the resulting mixture was refluxed for 5 h. After completion of the reaction, the solvent was evaporated, and the residue was washed with ethyl acetate and brine. The solvent was dried with anhydrous  $Na_2SO_4$  and removed under reduced pressure. The crude product was purified by column chromatography using basic alumina. Elution with EtOAc/hexane (1:9 v/v) yielded ethyl 5-(prop-2-yn-1-ylamino)-1-naphthoate (5) as a yellow oil (0.120 g, 54%).

$^1H$  NMR ( $CDCl_3$ , 400 MHz):  $\delta$  8.29 (d, 1H,  $H_{naphthalene}$ ,  $J = 8.8$  Hz), 8.09 (d, 1H,  $H_{naphthalene}$ ,  $J = 6.8$  Hz), 7.9 (d, 1H,  $H_{naphthalene}$ ,  $J = 8.4$  Hz), 7.49 (t, 1H,  $H_{naphthalene}$ ,  $J = 8.4$  Hz), 7.43–7.39 (m, 1H,  $H_{naphthalene}$ ), 6.76 (d, 1H,  $H_{naphthalene}$ ,  $J = 7.6$  Hz), 4.57 (s, 1H, NH), 4.47 (q, 2H,  $OCH_2$ ), 4.08 (d, 2H,  $NCH_2$ ,  $J = 2$  Hz), 2.29 (t, 1H,  $CH_{alkyne}$ ,  $J = 2.4$  Hz), 1.45 (t, 3H,  $CH_3$ ,  $J = 7.2$  Hz).  $^{13}C$  NMR ( $CDCl_3$ , 100 MHz):  $\delta$  168.1, 142.4, 132.1, 129.6, 128.5, 128.2, 124.7, 124.4, 123.5, 116.3, 106.2, 80.7, 71.8, 61.1, 33.0, 14.4. ESI-MS,  $m/z$  (relative intensity): 254 ( $M^+ + 1$ ). Anal. Calcd for  $C_{16}H_{15}O_2N$ : C, 75.87; H, 5.97; N, 5.53. Found: C, 75.58; H, 5.78; N, 5.34.

**Synthesis of Compound 6.** A solution of compound 5 (0.170 g, 0.672 mmol) and 0.9 equiv of azidomethylferrocene (0.146 g, 0.605

mmol) in dry DMF was made in a Schlenk flask equipped with a stirrer bar and degassed for 45 min.  $CuI$  (0.4 equiv) and DBU (0.6 equiv) were added, and the resulting solution was heated at  $60^\circ C$  for 4 h. The reaction mixture was diluted with dichloromethane, followed by excess methanol/water (1:1 v/v) solution. The organic phase was separated and dried over  $Na_2SO_4$ , and the solvent was removed under reduced pressure. The crude residue was purified by column chromatography using silica gel. Elution with EtOAc/hexane (2:8 v/v) yielded 6 as a yellow solid (0.250 g, 75%).

$^1H$  NMR ( $CDCl_3$ , 400 MHz):  $\delta$  8.77 (d, 1H,  $H_{naphthalene}$ ,  $J = 8.4$  Hz), 8.71 (s, 1H, CH), 8.48 (d, 1H,  $H_{naphthalene}$ ,  $J = 8.8$  Hz), 8.20–8.18 (m, 1H,  $H_{naphthalene}$ ), 8.13 (s, 1H,  $H_{triazole}$ ), 7.60–7.56 (m, 1H,  $H_{naphthalene}$ ), 7.51–7.47 (m, 1H,  $H_{naphthalene}$ ), 7.10 (d, 1H,  $H_{naphthalene}$ ,  $J = 7.6$  Hz), 5.41 (s, 2H,  $NCH_2$ ), 4.47 (q, 2H,  $OCH_2$ ), 4.36 (t, 2H,  $H_{Cp}$ ,  $J = 1.6$  Hz), 4.28 (t, 2H,  $H_{Cp}$ ,  $J = 1.6$  Hz), 4.23 (s, 5H,  $H_{Cp}$ ), 1.46 (t, 3H,  $OCH_2CH_3$ ).  $^{13}C$  NMR ( $CDCl_3$ , 100 MHz):  $\delta$  167.9, 152.8, 148.9, 131.8, 130.6, 129.2, 128.9, 128.0, 127.6, 124.5, 124.2, 122.8, 114.6, 113.3, 80.2, 69.5, 69.2, 69.1, 61.2, 50.6, 29.8, 14.5. Mp: 106–108  $^\circ C$ . ESI-MS,  $m/z$  (relative intensity): 493 ( $M^+ + 1$ ). Anal. Calcd for  $C_{27}H_{24}FeN_4O_2$ : C, 65.87; H, 4.91; N, 11.38. Found: C, 65.69; H, 5.08; N, 11.14.

**X-ray Crystallographic Analysis.** X-ray-quality crystals of 6 were grown by slow diffusion of a hexane/EtOAc (4:6 v/v) solution. The intensity data were collected on a Super Nova, Dual, Cu at zero, Eos diffractometer. The crystal was kept at 100.00(10) K during data collection. With OLEX2,<sup>44</sup> the structure was solved with the Superflip<sup>45</sup> structure solution program using charge flipping and refined with the SHELXL<sup>46</sup> refinement package and least-squares minimization. The hydrogen atoms were refined isotropically at calculated positions using a riding model. CCDC 1543246 contains the supplementary crystallographic data for this paper. These data can be obtained free of charge from the Cambridge Crystallographic Data Centre via [www.ccdc.cam.ac.uk/data\\_request/cif](http://www.ccdc.cam.ac.uk/data_request/cif).

**Crystal Data for 6.** Formula,  $C_{27}H_{24}FeN_4O_2$ ; crystal system, monoclinic; space group,  $P2_1/c$ ; unit cell dimensions,  $a = 13.7802(4)$  Å,  $b = 9.5136(3)$  Å,  $c = 17.4606(5)$  Å,  $\beta = 90.693(2)^\circ$ ;  $Z = 4$ ; density (calcd) =  $1.429 mg/m^3$ ;  $R_{int} = 0.0217$ ; final R indices [ $I > 2\sigma(I)$ ],  $R_1 = 0.0370$ ;  $wR_2 = 0.0791$ ;  $\theta$  range (deg), 2.33–27.46; total reflection collected, 4600; independent reflections, 3917; goodness of fit on  $F^2 = 1.098$ .

**Computational Details.** All of the calculations (DFT and TD-DFT) were carried out with the Gaussian 09 program package (revision C.01).<sup>47</sup> The ground-state geometries were optimized without symmetry constraints using the hybrid Becke–Lee–Yang–Parr (B3LYP) functional<sup>48</sup> in combination with the def2-SVP basis set<sup>49</sup> from the EMSL Basis Set Exchange Library. The 60 core electrons of mercury were replaced by the quasi-relativistic effective core potential def2-ECP.<sup>50</sup> The model compounds were fully optimized in the gas phase (no solvent effect). The crystallographic coordinates of 6 were used as a starting geometry for complete geometry optimization. Frequency calculations were performed in order to verify the nature of the stationary state as a minimum, which was confirmed by the absence of any imaginary frequency. The energy values provided herein contain zero-point energy (ZPE) corrections. The lowest-energy gas-phase vertical transitions were calculated (singlets, 15 states) on the structures optimized by TD-DFT using the Coulomb-attenuated functional cam-B3LYP<sup>51</sup> in combination with the def2-SVP basis set. The cam-B3LYP functional was selected because it has been shown to be effective for ICT systems.<sup>52</sup> With the optimized ground-state ( $S_0$ ) geometry as the starting coordinate, TD-DFT geometry optimization of the  $S_1$  state of 6 was performed. Additionally, TD-DFT cam-B3LYP/6-31G(d)  $S_1$  optimization of 6 was conducted with inclusion of acetonitrile solvation using the polarizable continuum model. Natural bonding analyses were performed with the natural bond orbital (NBO) partitioning scheme<sup>53</sup> as implemented in Gaussian 09. Wiberg bond index values<sup>54</sup> were obtained by NBO analysis. To understand the nature of the bonding of 6 and  $[6-Hg^{2+}]$  further, the topological properties of the resultant electron density,  $\rho$ , obtained from the wave functions of all of the optimized structures were analyzed with the quantum theory of atoms

in molecules (QTAIM).<sup>55</sup> The QTAIM analysis was carried out utilizing the Multiwfn V.3.3.8 package,<sup>56</sup> whereas the wave functions were generated with Gaussian 09 at the same level of theory as was used for geometry optimization.

## ■ ASSOCIATED CONTENT

### ● Supporting Information

The Supporting Information is available free of charge on the ACS Publications website at DOI: 10.1021/acs.inorgchem.7b01304.

<sup>1</sup>H, <sup>13</sup>C, and ESI-MS data for compounds **4**, **4b**, **4c**, **5**, and **6**; UV-vis spectra and fluorescence spectra upon titration with different metal ions; ESI-MS spectrum of [6·Hg<sup>2+</sup>]; Job plot; detailed computational studies (PDF)

### Accession Codes

CCDC 1543246 contains the supplementary crystallographic data for this paper. These data can be obtained free of charge via [www.ccdc.cam.ac.uk/data\\_request/cif](http://www.ccdc.cam.ac.uk/data_request/cif), or by e-mailing [data\\_request@ccdc.cam.ac.uk](mailto:data_request@ccdc.cam.ac.uk), or by contacting The Cambridge Crystallographic Data Centre, 12 Union Road, Cambridge CB2 1EZ, U.K.; fax: +44 1223 336033.

## ■ AUTHOR INFORMATION

### Corresponding Author

\*E-mail: [thakura@nitrrkl.ac.in](mailto:thakura@nitrrkl.ac.in), [babuiitm07@gmail.com](mailto:babuiitm07@gmail.com). Phone: +918895012676.

### ORCID

Arunabha Thakur: 0000-0003-4577-3683

### Present Address

<sup>1</sup>Department of Chemistry, Jadavpur University, Kolkata-700032, India

### Notes

The authors declare no competing financial interest.

## ■ ACKNOWLEDGMENTS

Generous support from the Department of Science and Technology (DST), New Delhi (an Inspire Faculty Fellowship) is gratefully acknowledged.

## ■ REFERENCES

- (1) (a) Ge, L.; Wang, W.; Sun, X.; Hou, T.; Li, F. Versatile and Programmable DNA Logic Gates on Universal and Label-Free Homogeneous Electrochemical Platform. *Anal. Chem.* **2016**, *88*, 9691–9698. (b) Pischel, U. Chemical Approaches to Molecular Logic Elements for Addition and Subtraction. *Angew. Chem., Int. Ed.* **2007**, *46*, 4026–4040.
- (2) de Silva, A. P.; Uchiyama, S. Molecular Logic and Computing. *Nat. Nanotechnol.* **2007**, *2*, 399–410.
- (3) (a) Wang, B.; Buck, M. Rapid Engineering of Versatile Molecular Logic Gates using Heterologous Genetic Transcriptional Modules. *Chem. Commun.* **2014**, *50*, 11642–11644. (b) Raymo, F. M. Digital Processing and Communication with Molecular Switches. *Adv. Mater.* **2002**, *14*, 401–414.
- (4) Szaciłowski, K. Digital Information Processing in Molecular System. *Chem. Rev.* **2008**, *108*, 3481–3548.
- (5) de Silva, A. P.; Gunaratne, H. Q. N.; McCoy, C. P. A Molecular Photoionic AND Gate Based on Fluorescence Signalling. *Nature* **1993**, *364*, 42–44.
- (6) Katz, E.; Privman, V. Enzyme-Based Logic Systems for Information Processing. *Chem. Soc. Rev.* **2010**, *39*, 1835–1857.
- (7) (a) Andréasson, J.; Pischel, U. Smart Molecules at Work-Mimicking Advanced Logic Operations. *Chem. Soc. Rev.* **2010**, *39*, 174–188. (b) Tian, H. Data Processing on a Unimolecular Platform. *Angew. Chem., Int. Ed.* **2010**, *49*, 4710–4712.
- (8) Credi, A. Molecules That Make Decisions. *Angew. Chem., Int. Ed.* **2007**, *46*, 5472–5475.
- (9) de Silva, A. P. Molecular Logic Gate Arrays. *Chem. - Asian J.* **2011**, *6*, 750–766.
- (10) Magri, D. C.; Fava, M. C.; Mallia, C. J. A Sodium-Enabled 'Pourbaix Sensor': A Three-Input AND Logic Gate as a 'lab-on-a-molecule' for Monitoring Na<sup>+</sup>, pH and pE. *Chem. Commun.* **2014**, *50*, 1009–1011.
- (11) de Ruiter, G.; van der Boom, M. E. Surface-Confined Assemblies and Polymers for Molecular Logic. *Acc. Chem. Res.* **2011**, *44*, 563–573.
- (12) (a) Li, W.; Yang, Y.; Yan, H.; Liu, Y. Three-Input Majority Logic Gate and Multiple Input Logic Circuit Based on DNA Strand Displacement. *Nano Lett.* **2013**, *13*, 2980–2988. (b) de Silva, A. P.; McClenaghan, N. D. Simultaneously Multiply-Configurable or Superposed Molecular Logic Systems Composed of ICT (Internal Charge Transfer) Chromophores and Fluorophores Integrated with One- or Two-Ion Receptors. *Chem. - Eur. J.* **2002**, *8*, 4935–4945.
- (13) (a) Chen, C.; Zhao, D.; Sun, J.; Yang, X. Colorimetric Logic Gate for Pyrophosphate and Pyrophosphatase via Regulating the Catalytic Capability of Horseradish Peroxidase. *ACS Appl. Mater. Interfaces* **2016**, *8*, 29529–29535. (b) Pita, M.; Katz, E. Multiple Logic Gates Based on Electrically Wired Surface-Reconstituted Enzymes. *J. Am. Chem. Soc.* **2008**, *130*, 36–37.
- (14) (a) You, M.; Zhu, G.; Chen, T.; Donovan, M. J.; Tan, W. Programmable and Multiparameter DNA-Based Logic Platform For Cancer Recognition and Targeted Therapy. *J. Am. Chem. Soc.* **2015**, *137*, 667–674. (b) Angelos, S.; Khashab, N. M.; Yang, Y.-W.; Trabolsi, A.; Khatib, H. A.; Stoddart, J. F.; Zink, J. I. pH Clock-Operated Mechanized Nanoparticles. *J. Am. Chem. Soc.* **2009**, *131*, 12912–12914.
- (15) Fratto, B. E.; Roby, L. J.; Guz, N.; Katz, E. Enzyme-Based Logic Gates Switchable Between OR, NXOR and NAND Boolean Operations Realized in a Flow System. *Chem. Commun.* **2014**, *50*, 12043–12046.
- (16) (a) Li, Y.; Li, W.; He, K.-Y.; Li, P.; Huang, Y.; Nie, Z.; Yao, S.-Z. A Biomimetic Colorimetric Logic Gate System Based on Multi-Functional Peptide-Mediated Gold Nano particle Assembly. *Nanoscale* **2016**, *8*, 8591–8599. (b) de Ruiter, G.; Motiei, L.; Choudhury, J.; Oded, N.; van der Boom, M. E. Electrically Addressable Multistate Volatile Memory with Flip-Flop and Flip-Flap-Flop Logic Circuits on a Solid Support. *Angew. Chem.* **2010**, *122*, 4890–4893.
- (17) (a) Hettie, K. S.; Klockow, J. L.; Glass, T. E. Three-Input Logic Gates with Potential Applications for Neuronal Imaging. *J. Am. Chem. Soc.* **2014**, *136*, 4877–4880. (b) Andréasson, J.; Straight, S. D.; Moore, T. A.; Moore, A. L.; Gust, D. Molecular All-Photonic Encoder-Decoder. *J. Am. Chem. Soc.* **2008**, *130*, 11122–11128.
- (18) Konry, T.; Walt, D. R. Intelligent Medical Diagnostics via Molecular Logic. *J. Am. Chem. Soc.* **2009**, *131*, 13232–13233.
- (19) Kou, S.; Lee, H. N.; van Noort, D.; Swamy, K. M. K.; Kim, S. H.; Soh, J. H.; Lee, K.-M.; Nam, S.-W.; Yoon, J.; Park, S. Fluorescent Molecular Logic Gates Using Microfluidic Devices. *Angew. Chem., Int. Ed.* **2008**, *47*, 872–876.
- (20) Carter, K. P.; Young, A. M.; Palmer, A. E. Fluorescent Sensors for Measuring Metal Ions in Living Systems. *Chem. Rev.* **2014**, *114*, 4564–4601.
- (21) McClure, D. S. Spin-Orbit Interaction in Aromatic Molecules. *J. Chem. Phys.* **1952**, *20*, 682–685.
- (22) Varnes, A. W.; Dodson, R. B.; Wehry, E. L. Interactions of Transition-Metal Ions with Photoexcited States of Flavins. Fluorescence quenching studies. *J. Am. Chem. Soc.* **1972**, *94*, 946–950.
- (23) (a) Gunnlaugsson, T.; Davis, A. P.; O'Brien, J. E.; Glynn, M. Fluorescent Sensing of Pyrophosphate and Bis-carboxylates with Charge Neutral PET Chemosensors. *Org. Lett.* **2002**, *4*, 2449–2452. (b) Vance, D. H.; Czarnik, A. W. Real-Time Assay of Inorganic Pyrophosphatase Using a High-Affinity Chelation-Enhanced Fluorescence Chemosensor. *J. Am. Chem. Soc.* **1994**, *116*, 9397–9398.

- (c) Kim, S. K.; Yoon, J. A New Fluorescent PET Chemosensor for Fluoride Ions. *Chem. Commun.* **2002**, 7, 770–771. (d) Zhu, J.; Sun, S.; Jiang, K.; Wang, Y.; Liu, W.; Lin, H. A Highly Sensitive and Selective Fluorimetric Probe for Intracellular Peroxynitrite Based on Photo-induced Electron Transfer from Ferrocene to Carbon dots. *Biosens. Bioelectron.* **2017**, 97, 150–156. (e) Cheng, R.; Peng, Y.; Ge, C.; Bu, Y.; Liu, H.; Huang, H.; Ou, S.; Xue, Y.; Dai, L. A Turn-on Fluorescent Lysine Nanoprobe Based On the Use of the Alizarin Red Aluminum(III) Complex Conjugated to Graphene Oxide, and Its Application to Cellular Imaging of Lysine. *Microchim. Acta* **2017**, 184, 3521–3528.
- (24) (a) Beer, P. D. Transition-Metal Receptor Systems for the Selective Recognition and Sensing of Anionic Guest Species. *Acc. Chem. Res.* **1998**, 31, 71–80. (b) Kim, M.-J.; Konduri, R.; Ye, H.; MacDonnell, F. M.; Puntoriero, F.; Serroni, S.; Campagna, S.; Holder, T.; Kinsel, G.; Rajeshwar, K. Dinuclear Ruthenium(II) Polypyridyl Complexes Containing Large, Redox-Active, Aromatic Bridging Ligands: Synthesis, Characterization, and Intramolecular Quenching of MLCT Excited States. *Inorg. Chem.* **2002**, 41, 2471–2476. (c) Frin, K. P. M.; de Almeida, R. M. Mono- and Di-nuclear Re(I) Complexes and The Role of Protonable Nitrogen Atoms in Quenching Emission by Hydroquinone. *Photochem. Photobiol. Sci.* **2017**, 16, 1230–1237. (d) Coe, B. J.; Harris, J. A.; Brunschwig, B. S.; Asselberghs, I.; Clays, K.; Garin, J.; Orduna, J. Three-Dimensional Nonlinear Optical Chromophores Based on Metal-to-Ligand Charge-Transfer from Ruthenium(II) or Iron(II) Centers. *J. Am. Chem. Soc.* **2005**, 127, 13399–13410.
- (25) (a) Xu, Z.; Xiao, Y.; Qian, X.; Cui, J.; Cui, D. Ratiometric and Selective Fluorescent Sensor for Cu<sup>II</sup> Based on Internal Charge Transfer (ICT). *Org. Lett.* **2005**, 7, 889–892. (b) Wu, F.-Y.; Jiang, Y.-B. *p*-Dimethylaminobenzamide as an ICT Dual Fluorescent Neutral Receptor for Anions under Proton Coupled Electron Transfer Sensing Mechanism. *Chem. Phys. Lett.* **2002**, 355, 438–444. (c) Bhat, H. R.; Jha, P. C. A Theoretical Study on Anion Sensing Mechanism of Multi-Phosphonium Triarylboranes: Intramolecular Charge Transfer and Configurational Changes. *Phys. Chem. Chem. Phys.* **2017**, 19, 14811–14820. (d) Liu, X.; Su, Y.; Tian, H.; Yang, L.; Zhang, H.; Song, X.; Foley, J. W. Ratiometric Fluorescent Probe for Lysosomal pH Measurement and Imaging in Living Cells Using Single-Wavelength Excitation. *Anal. Chem.* **2017**, 89, 7038–7045. (e) Liu, X.; Cole, J. M.; Xu, Z. Substantial Intramolecular Charge Transfer Induces Long Emission Wavelengths and Mega Stokes Shifts in 6-Aminocoumarins. *J. Phys. Chem. C* **2017**, 121, 13274–13279.
- (26) (a) Nishizawa, S.; Kato, Y.; Teramae, N. Fluorescence Sensing of Anions via Intramolecular Excimer Formation in a Pyrophosphate-Induced Self-Assembly of a Pyrene-Functionalized Guanidinium Receptor. *J. Am. Chem. Soc.* **1999**, 121, 9463–9464. (b) Yuasa, H.; Miyagawa, N.; Izumi, T.; Nakatani, M.; Izumi, M.; Hashimoto, H. Hinge Sugar as a Movable Component of an Excimer Fluorescence Sensor. *Org. Lett.* **2004**, 6, 1489–1492. (c) Schazmann, B.; Alhashimy, N.; Diamond, D. Chloride Selective Calix[4]arene Optical Sensor Combining Urea Functionality with Pyrene Excimer Transduction. *J. Am. Chem. Soc.* **2006**, 128, 8607–8614. (d) Bai, Y.; Zhao, Q. Rapid Fluorescent Detection of Immunoglobulin E Using an Aptamer Switch Based on Binding-Induced Pyrene Excimer. *Anal. Methods* **2017**, 9, 3962–3967. (e) Martelo, L.; Fedorov, A.; Berberan-Santos, M. N. Monomer-Excimer Mixed Fluorescence Decays in the Phasor Space. *J. Lumin.* **2017**, 192, 64–70.
- (27) (a) Zhang, X.; Guo, L.; Wu, F.-Y.; Jiang, Y.-B. Development of Fluorescent Sensing of Anions under Excited-State Intermolecular Proton Transfer Signaling Mechanism. *Org. Lett.* **2003**, 5, 2667–2670. (b) Oscar, B. G.; Liu, W.; Rozanov, N. D.; Fang, C. Ultrafast Intermolecular Proton Transfer to Proton Scavenger in an Organic Solvent. *Phys. Chem. Chem. Phys.* **2016**, 18, 26151–26160. (c) Heo, W.; Uddin, N.; Park, J. W.; Rhee, Y. M.; Choi, C. H.; Joo, T. Coherent Intermolecular Proton Transfer in the Acid-Base Reaction of Excited State Pyranine. *Phys. Chem. Chem. Phys.* **2017**, 19, 18243–18251.
- (28) Wu, J.; Liu, W.; Ge, J.; Zhang, H.; Wang, P. New Sensing Mechanisms for Design of Fluorescent Chemosensors Emerging in Recent Years. *Chem. Soc. Rev.* **2011**, 40, 3483–3495.
- (29) (a) Wu, J.-S.; Liu, W.-M.; Zhuang, X.-Q.; Wang, F.; Wang, P.-F.; Tao, S.-L.; Zhang, X.-H.; Wu, S.-K.; Lee, S.-T. Fluorescence Turn On of Coumarin Derivatives by Metal Cations: A New Signaling Mechanism Based on C=N Isomerization. *Org. Lett.* **2007**, 9, 33–36. (b) Ray, D.; Bharadwaj, P. K. A Coumarin-Derived Fluorescence Probe Selective for Magnesium. *Inorg. Chem.* **2008**, 47, 2252–2254.
- (30) Sun, Y.-Q.; Wang, P.; Liu, J.; Zhang, J.; Guo, W. A Fluorescent Turn-On Probe for Bisulfite Based on Hydrogen Bond-Inhibited C=N Isomerization Mechanism. *Analyst* **2012**, 137, 3430–3433.
- (31) (a) Zapata, F.; Caballero, A.; Espinosa, A.; Tárraga, A.; Molina, P. A Selective Redox and Chromogenic Probe for Hg(II) in Aqueous Environment Based on a Ferrocene-Azaquinoxaline Dyad. *Inorg. Chem.* **2009**, 48, 11566–11575. (b) Alfonso, M.; Sola, A.; Caballero, A.; Tárraga, A.; Molina, P. Heteroditopic Ligands Based on Ferrocenyl Benzimidazoles Fused to an Additional Diaza Heterocyclic Ring System. *Dalton Trans.* **2009**, 43, 9653–9658. (c) Zapata, F.; Caballero, A.; Molina, P.; Tárraga, A. A Ferrocene-Quinoxaline Derivative as a Highly Selective Probe for Colorimetric and Redox Sensing of Toxic Mercury(II) Cations. *Sensors* **2010**, 10, 11311–11321.
- (32) (a) Thakur, A.; Mandal, D.; Ghosh, S. Sensitive and Selective Redox, Chromogenic, and “Turn-On” Fluorescent Probe for Pb(II) in Aqueous Environment. *Anal. Chem.* **2013**, 85, 1665–1674. (b) Bhatta, S. R.; Bheemireddy, V.; Vijaykumar, G.; Thakur, A. Triazole Appended Mono and 1,1′ Di-Substituted Ferrocene-Naphthalene Conjugates: Highly Selective and Sensitive Multi-Responsive Probes for Hg(II). *Sens. Actuators, B* **2017**, 240, 640–650. (c) Thakur, A.; Adarsh, N. N.; Chakraborty, A.; Devi, M.; Ghosh, S. Synthesis of Mono and Doubly Alkynyl Substituted Ferrocene and Its Crystal Engineering using C–H⋯O Supramolecular Synthons. *J. Organomet. Chem.* **2010**, 695, 1059–1064. (d) Thakur, A.; Ghosh, S. An Efficient Ferrocene Derivative as a Chromogenic, Optical, and Electrochemical Receptor for Selective Recognition of Mercury(II) in an Aqueous Environment. *Organometallics* **2012**, 31, 819–826. (e) Bhatta, S. R.; Bheemireddy, V.; Thakur, A. A Redox-Driven Fluorescence “Off–On” Molecular Switch Based on a 1,1′-Unsymmetrically Substituted Ferrocenyl Coumarin System: Mimicking Combinational Logic Operation. *Organometallics* **2017**, 36, 829–838.
- (33) Thakur, A.; Sardar, S.; Ghosh, S. A Highly Selective Redox, Chromogenic, and Fluorescent Chemosensor for Hg<sup>2+</sup> in Aqueous Solution Based on Ferrocene–Glycine Bioconjugates. *Inorg. Chem.* **2011**, 50, 7066–7073.
- (34) (a) Guo, X.; Qian, X.; Jia, L. A Highly Selective and Sensitive Fluorescent Chemosensor for Hg<sup>2+</sup> in Neutral Buffer Aqueous Solution. *J. Am. Chem. Soc.* **2004**, 126, 2272–2273. (b) Xu, Z.; Xiao, Y.; Qian, X.; Cui, J.; Cui, D. Ratiometric and Selective Fluorescent Sensor for Cu<sup>II</sup> Based on Internal Charge Transfer (ICT). *Org. Lett.* **2005**, 7, 889–892. (c) Xu, Z.; Qian, X.; Cui, J. Colorimetric and Ratiometric Fluorescent Chemosensor with a Large Red-Shift in Emission: Cu(II)-Only Sensing by Deprotonation of Secondary Amines as Receptor Conjugated to Naphthalimide Fluorophore. *Org. Lett.* **2005**, 7, 3029–3032.
- (35) (a) Banthia, S.; Samanta, A. Influence of Structure on the Unusual Spectral Behavior of 4-dialkylamino-1, 8-naphthalimide. *Chem. Lett.* **2005**, 34, 722–723. (b) de Silva, A. P.; Gunaratne, H. Q. N.; Habib-Jiwan, J.-L.; McCoy, C. P.; Rice, T. E.; Soumillion, J.-P. New Fluorescent Model Compounds for the Study of Photoinduced Electron Transfer: The Influence of a Molecular Electric Field in the Excited State. *Angew. Chem., Int. Ed.* **1995**, 34, 1728–1731.
- (36) (a) Li, Y.; Cao, L.; Tian, H. Fluoride Ion-Triggered Dual Fluorescence Switch Based on Naphthalimides Winged Zinc Porphyrin. *J. Org. Chem.* **2006**, 71, 8279–8282. (b) Esteban-Gómez, D.; Fabbri, L.; Licchelli, M. Why, on Interaction of Urea-Based Receptors with Fluoride, Beautiful Colors Develop. *J. Org. Chem.* **2005**, 70, 5717–5720. (c) Liu, B.; Tian, H. A Ratiometric Fluorescent Chemosensor for Fluoride Ions Based on a Proton Transfer Signaling Mechanism. *J. Mater. Chem.* **2005**, 15, 2681–2686.

- (37) (a) de Silva, A. P.; Gunaratne, H. Q. N.; Gunnlaugsson, T.; Huxley, A. J. M.; McCoy, C. P.; Rademacher, J. T.; Rice, T. E. Signaling Recognition Events with Fluorescent Sensors and Switches. *Chem. Rev.* **1997**, *97*, 1515–1566. (b) de Silva, A. P.; Fox, D. B.; Huxley, A. J. M.; Moody, T. M. Combining Luminescence, Coordination and Electron Transfer for Signalling Purposes. *Coord. Chem. Rev.* **2000**, *205*, 41–57.
- (38) Mallick, A.; Chattopadhyay, N. Photophysics in Motionally constrained Bioenvironment: Interactions of Norharmane with Bovine Serum Albumin. *Photochem. Photobiol.* **2005**, *81*, 419–424.
- (39) Benesi, H. A.; Hildebrand, J. H. A Spectrophotometric Investigation of the Interaction of Iodine with Aromatic Hydrocarbons. *J. Am. Chem. Soc.* **1949**, *71*, 2703–2707.
- (40) Wang, P.; Liu, J.; Lv, X.; Liu, Y.; Zhao, Y.; Guo, W. A Naphthalimide-Based Glyoxal Hydrazone for Selective Fluorescence Turn-On Sensing of Cys and Hcy. *Org. Lett.* **2012**, *14*, 520–523.
- (41) (a) González, M. C.; Otón, F.; Orenes, R. A.; Espinosa, A.; Tárraga, A.; Molina, P. Ferrocene-Triazole-Pyrene Triads as Multi-channel Heteroditopic Recognition Receptors for Anions, Cations and Ion Pairs. *Organometallics* **2014**, *33*, 2837–2852. (b) Romero, T.; Orenes, R. A.; Espinosa, A.; Tárraga, A.; Molina, P. Synthesis, Structural Characterization, and Electrochemical and Optical Properties of Ferrocene-Triazole-Pyridine Triads. *Inorg. Chem.* **2011**, *50*, 8214–8224. (c) Wang, X.-L.; Wan, K.; Zhou, C.-H. Synthesis of novel sulfanilamide-derived 1,2,3-triazoles and their evaluation for anti-bacterial and antifungal activities. *Eur. J. Med. Chem.* **2010**, *45*, 4631–4639.
- (42) Pérez-Balderas, F.; Ortega-Muñoz, M.; Morales-Sanfrutos, J.; Hernández-Mateo, F.; Calvo-Flores, F. G.; Calvo-Asín, J. A.; Isac-García, J.; Santoyo-González, F. Multivalent Neoglycoconjugates by Regiospecific Cycloaddition of Alkynes and Azides Using Organic-Soluble Copper Catalysts. *Org. Lett.* **2003**, *5*, 1951–1954.
- (43) Casas-Solvas, J. M.; Vargas-Berenguel, A.; Capitán-Vallvey, L. F.; Santoyo-González, F. Convenient Methods for the Synthesis of Ferrocene-Carbohydrate Conjugates. *Org. Lett.* **2004**, *6*, 3687–3690.
- (44) Dolomanov, O. V.; Bourhis, L. J.; Gildea, R. J.; Howard, J. A. K.; Puschmann, H. OLEX2: A Complete Structure Solution, Refinement and Analysis Program. *J. Appl. Crystallogr.* **2009**, *42*, 339–341.
- (45) Palatinus, L.; Chapuis, G. SUPERFLIP- A Computer Program for the Solution of Crystal Structures by Charge Flipping in Arbitrary Dimensions. *J. Appl. Crystallogr.* **2007**, *40*, 786–790.
- (46) Sheldrick, G. M. A Short History of SHELX. *Acta Crystallogr., Sect. A: Found. Crystallogr.* **2008**, *64*, 112–122.
- (47) Frisch, M. J.; Trucks, G. W.; Schlegel, H. B.; Scuseria, G. E.; Robb, M. A.; Cheeseman, J. R.; Scalmani, G.; Barone, V.; Mennucci, B.; Petersson, G. A.; Nakatsuji, H.; Caricato, M.; Li, X.; Hratchian, H. P.; Izmaylov, A. F.; Bloino, J.; Zheng, G.; Sonnenberg, J. L.; Hada, M.; Ehara, M.; Toyota, K.; Fukuda, R.; Hasegawa, J.; Ishida, M.; Nakajima, T.; Honda, Y.; Kitao, O.; Nakai, H.; Vreven, T.; Montgomery, J. A., Jr.; Peralta, J. E.; Ogliaro, F.; Bearpark, M.; Heyd, J. J.; Brothers, E.; Kudin, K. N.; Staroverov, V. N.; Kobayashi, R.; Normand, J.; Raghavachari, K.; Rendell, A.; Burant, J. C.; Iyengar, S. S.; Tomasi, J.; Cossi, M.; Rega, N.; Millam, J. M.; Klene, M.; Knox, J. E.; Cross, J. B.; Bakken, V.; Adamo, C.; Jaramillo, J.; Gomperts, R.; Stratmann, R. E.; Yazyev, O.; Austin, A. J.; Cammi, R.; Pomelli, C.; Ochterski, J. W.; Martin, R. L.; Morokuma, K.; Zakrzewski, V. G.; Voth, G. A.; Salvador, P.; Dannenberg, J. J.; Dapprich, S.; Daniels, A. D.; Farkas, Ö.; Foresman, J. B.; Ortiz, J. V.; Cioslowski, J.; Fox, D. J. *Gaussian 09*, revision C.01; Gaussian, Inc.: Wallingford, CT, 2009.
- (48) (a) Becke, A. D. Density-Functional Exchange-Energy Approximation with Correct Asymptotic Behavior. *Phys. Rev. A: At., Mol., Opt. Phys.* **1988**, *38*, 3098–3100. (b) Lee, C.; Yang, W.; Parr, R. G. Development of the Colle-Salvetti Correlation-Energy Formula into a Functional of the Electron Density. *Phys. Rev. B: Condens. Matter Mater. Phys.* **1988**, *37*, 785–789. (c) Becke, A. D. Density-Functional Thermochemistry. III. The role of exact exchange. *J. Chem. Phys.* **1993**, *98*, 5648–5652.
- (49) Weigend, F.; Ahlrichs, R. Balanced Basis Sets of Split Valence, Triple Zeta Valence and Quadruple Zeta Valence Quality for H to Rn: Design and Assessment of Accuracy. *Phys. Chem. Chem. Phys.* **2005**, *7*, 3297–3305.
- (50) Andrae, D.; Häußermann, U.; Dolg, M.; Stoll, H.; Preuß, H. Energy-Adjusted *ab initio* Pseudopotentials for the Second and Third Row Transition Elements. *Theor. Chim. Acta* **1990**, *77*, 123–141.
- (51) Yanai, T.; Tew, D. P.; Handy, N. C. A New Hybrid Exchange-Correlation Functional Using the Coulomb-Attenuating Method (CAM-B3LYP). *Chem. Phys. Lett.* **2004**, *393*, 51–57.
- (52) (a) Preat, J. Photoinduced Energy-Transfer and Electron-Transfer Processes in Dye-Sensitized Solar Cells: TDDFT Insights for Triphenylamine Dyes. *J. Phys. Chem. C* **2010**, *114*, 16716–16725. (b) Wiggins, P.; Williams, J. A.; Tozer, D. J. Excited State Surfaces in Density Functional Theory: A New Twist on an Old Problem. *J. Chem. Phys.* **2009**, *131*, 091101–1–091101–4. (c) Peach, M. J. G.; Cohen, A. J.; Tozer, D. J. Influence of Coulomb-Attenuation on Exchange–Correlation Functional Quality. *Phys. Chem. Chem. Phys.* **2006**, *8*, 4543–4549.
- (53) (a) Glendening, E. D.; Reed, A. E.; Carpenter, J. E.; Weinhold, F. *NBO 3.1*; University of Wisconsin: Madison, WI, 1988. (b) Reed, A. E.; Curtiss, L. A.; Weinhold, F. Intermolecular Interactions from a Natural Bond Orbital, Donor-Acceptor Viewpoint. *Chem. Rev.* **1988**, *88*, 899–926. (c) Weinhold, F.; Landis, R. *Valency and Bonding: A Natural Bond Orbital Donor–Acceptor Perspective*; Cambridge University Press: Cambridge; U.K., 2005.
- (54) Wiberg, K. B. Application of the Pople-Santry-Segal CNDO Method to the Cyclopropylcarbiny and Cyclobutyl Cation and to Bicyclobutane. *Tetrahedron* **1968**, *24*, 1083–1096.
- (55) (a) Bader, R. F. W. *Atoms in Molecules: A Quantum Theory*; Oxford University Press: Oxford, U.K., 1990. (b) Bader, R. F. W. A Bond Path: A Universal Indicator of Bonded Interactions. *J. Phys. Chem. A* **1998**, *102*, 7314–7323. (c) Bader, R. F. W. A Quantum Theory of Molecular Structure and its Applications. *Chem. Rev.* **1991**, *91*, 893–928.
- (56) Lu, T.; Chen, F. Multiwfn: A Multifunctional Wave Function Analyzer. *J. Comput. Chem.* **2012**, *33*, 580–592.